A review of atmospheric individual particle analyses: Methodologies and applications in environmental research

Longyi Shao[1]*, Pengju Liu[1], Tim Jones[2], Shushen Yang[3], Wenhua Wang[1,4], Daizhou Zhang[5], Yaowei Li[1,6], Cheng-Xue Yang[7], Jiaoping Xing[1,8], Cong Hou[1,9], Mengyuan Zhang[1], Xiaolei Feng[1], Wenjun Li[1], Kelly BéruBé[10].

1 State Key Laboratory of Coal Resources and Safe Mining & College of Geoscience and Surveying Engineering, China University of Mining and Technology (Beijing), Beijing 100083, China

2 School of Earth and Environmental Sciences, Cardiff University, Cardiff, CF10, 3YE, Wales, UK

3 School of Energy & Environment Engineering, Zhongyuan University of Technology, Zhengzhou 450007, Henan, Peoples R China

4 School of Resources and Materials, Northeastern University at Qinhuangdao, Qinhuangdao, 066004, China

5 Faculty of Environmental and Symbiotic Sciences, Prefectural University of Kumamoto, Kumamoto 862-8502, Japan

6 Hebei Center for Ecological and Environmental Geology Research, Hebei GEO University, Shijiazhuang 050031, China

7 Institute of Earth Sciences, China University of Geosciences (Beijing), Beijing 100083, China

8 School of Forestry, Jiangxi Agricultural University, Nanchang, 330045, China

9 Hebei University of Economics and Business, Shijiazhuang 050061, Hebei, China

10 School of Biosciences, Cardiff University, Cardiff CF10 3AX, Wales, UK

Highlights

1. The techniques of individual particle analyses are summarized.
2. The classification systems of the individual particles are reviewed.
3. Possible sources of individual primary and secondary particles are discussed.
4. Application of individual particle analysis in the environmental research are introduced.

Graphical Abstract

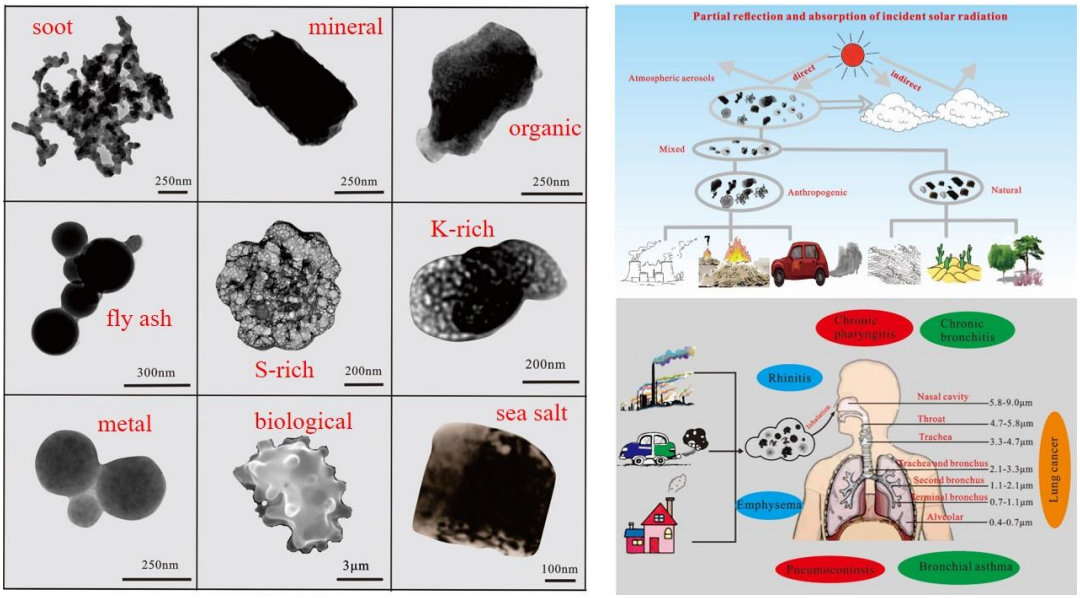

Abstract

Aerosol ultra-fine and nano-particles are playing essential roles in the evolution of the Earth environment because of their deep connections to the chemical conversions and solar radiation energy transfer in the atmosphere, and have also become an urgent public concern in recent years due to their adverse health effects. Electron microscopes, as major tools being able to accurately identify the physical and chemical characteristics of individual particles in micron and submicron size, have been widely used in aerosol studies, although some barriers remain for their low efficiency and high cost. In this work, current understandings on the physical and chemical characteristics, mixing state and heterogeneous chemical reactions of individual aerosol particles, mainly obtained with electron microscopes, are reviewed. First, the techniques of individual particle analyses are briefly summarized and their advantages and disadvantages are discussed. Then, the morphology and composition of major atmospheric particle types obtained with these techniques and how the information was used to identify particle sources are introduced. The effects of aerosol particles on the environment, climate, human health, and global geochemical cycles are also discussed based on the data from individual particle analyses. Finally, challenges faced in individual particle studies are prospected.

Keywords: climate, electron microscope, global geochemical cycles, health, individual particle analyses, particle source

1 Introduction

Airborne particulate matter is a general term for all types of solid and liquid particles in the atmosphere (Tang et al., 2006), which is an atmospheric pollutant that is potentially harmful to human health (Dockery et al., 1993). Aerosol in atmospheric science generally refers to the suspension system of solid particles, liquid particles, or both of them in a gaseous medium (Freney et al., 2010). PM_{10} refers to particulate matter in the ambient air that has an aerodynamic equivalent diameter of less than or equal to 10μm; also known as inhalable particulate matter. $PM_{2.5}$ refers to particulate matter in the ambient air that has an aerodynamic equivalent diameter of less than or equal to 2.5μm; also usually known as fine particulate matter (Jones et al., 2021). Ultrafine particle refers to particulate matter in the ambient air with an aerodynamic equivalent diameter of less than or equal to 0.1μm, also known as nanoparticles (Shao et al., 2000; Cao et al., 2014; Manigrasso et al., 2020; Naing and Lee, 2020). Atmospheric particulate matter is from natural and anthropogenic sources. Natural sources typically include emissions from crustal dust, wildfires, volcanic eruptions or resuspended volcanic ash, biological emission such as pollen and spores, and sea spray, in addition to particles produced via gas-to-particle conversions in the atmosphere (Li et al., 2016b; Oliveira et al., 2021; Trejos et al., 2021). The main anthropogenic sources include fuel combustion, industrial process, waste incineration and agricultural activity emissions (Silva et al., 2021). Atmospheric particulate matter released from anthropogenic sources is an important air pollutant (Chan and Yao, 2008; Bi et al., 2011). For example, industrial processes can emit large numbers of fugitive dust particles (Cheng et al., 2020); incineration of solid waste can release large numbers of soot particles (He et al., 2021); agricultural activities can emit large quantities of potassium-rich (K-rich) particles (Bi et al., 2011; Singh et al., 2018). The continuous accumulation of particles in the atmosphere and the increase of particle concentrations facilitate the formation of haze under certain meteorological conditions (Shen et al., 2021). Frequent haze events pose a significant threat to human health, even leading to increased numbers of mortality (Oberdorster et al., 1995; Pope et al., 1995; Garcia-

Hernandez et al., 2019). When particles are inhaled, they can cause a variety of health hazards including asthma, lung function decline and respiratory inflammation, and can also affect the cardiovascular, nervous, and immune systems (Daigle et al., 2003; Oberdorster et al., 2004; Pope and Dockery, 2006; Chai et al., 2019;). In addition, atmospheric particles can also directly or indirectly affect the climate. Sulfate particles reflect incident solar radiation (Krishnamohan et al., 2020); carbonaceous particles can absorb sunlight, leading to positive radiative forcing and global warming (McMeeking et al., 2011). Sea salt particles play a dual role in atmospheric radiation balance, scattering incoming solar radiation and absorbing ground radiation, thus directly affecting climate (Ayash et al., 2008; Meesang et al., 2013). At the same time, sea salt particles can also act as cloud condensation nuclei, indirectly affecting climate (Ayash et al., 2008). The absorption by brown carbon was noted to be highest in winter, accounting for 41% of the total absorption (Zhu et al., 2021). Another study found that sulfates and organic matter acted as coating materials enclosing the soot particles (Yuan et al., 2019), enhancing the light absorption capacity compared to the uncoated soot particles (Wang et al., 2017).

There are diverse research methods that can be applied to atmospheric particles. These methods are divided into bulk sample analysis and individual particle analysis. Bulk sample analysis has involved a variety of instrumental tests. Inductively Coupled Plasma Mass Spectrometer (ICP-MS) is a common method for bulk sample chemical composition analysis, which can be used to measure metal levels (Ari et al., 2020). Inductively Coupled Plasma-Optical Emission Spectroscopy (ICP-OES) is used to measure inorganic elements (Zalakeviciute et al., 2020). Ion Chromatograph (IC) is used to measure water-soluble ions (Rodriguez et al., 2020). Inductively Coupled Plasma Atomic Emission Spectrometry (ICP-AES) is used for the determination of elements in a great variety of different types of samples (Menzel et al., 2002). Additionally, bulk sample measurement methods include Aerosol Mass Spectrometry (AMS) (Reyes-Villegas et al., 2018), Elemental-Carbon tester, Meteorological Gas Chromatograph Mass Spectrometry (GC-MS) (Choi et al., 2020),

High Performance Liquid Chromatography Mass Spectrometry (HPLC/MS) (Buiarelli et al., 2018), and Proton Transfer Reaction Mass Spectrometry (PTR-MS) (Maji et al., 2020).

In bulk sample analysis, various instruments can simultaneously analyze hundreds or thousands of aerosol particles and characterize the mass concentrations of different components in the particles. These batch methods can quantify different aerosol species, depending on the instrument (Li et al., 2016b). However, bulk sample analysis has many limitations, they cannot provide mixing state and surface properties of airborne particles. The mixing state of particles is of great significance in the study of regional haze (Li et al., 2016b; Saikia et al., 2018). Due to the limitation of bulk sample analysis, individual particle analysis technology has been developed, which makes up for the deficiency of bulk sample analysis well.

Individual particle analysis was first used to analyze aerosol particles with an electron microscope in 1967 (Frank and Lodge, 1967). Bigg et al. (1974) developed vapour-deposited thin film method to test sulfate particle under electron microscope. Ayers et al. (1977) improved this method in 1977. With the development of measurement technology, microanalysis technology has been applied to the study of individual aerosol particle in the atmosphere. Ramsden and Shibaoka, (1982) studied the morphology and chemical composition of soot particles by scanning electron microscopy, transmission electron microscopy and EPMA (Electron Probe X-ray Micro-Analysis). Iwasaka et al. (1988) observed the morphology of individual particles in the height range from near the ground to about 4400m with electron microscope and found that particles were very frequently transported from Asian desert areas to the islands of Japan in the middle troposphere. In 1990s, many references on individual particle analysis have emerged. Individual particle analysis techniques began to be applied to mineralogy, morphology, chemical composition, and the relationship between various effects of particulate matter. Liu et al. (1994) analyzed atmospheric particulate matter in Qingdao and found that the sources of particulate matter mainly included soil dust, coal burning, cement industry, fuel oil and steel industry. Prospero

et al. (1999) studied the long-distance transport of sand dust in the southeastern United States affected by African dust storms and concluded that kaolinite is mainly located in low latitudes in West Africa, while illite is mainly located in northern regions to the Mediterranean coast. Zhang et al. (1998) made a preliminary classification of the morphology of particles, and analyzed individual sulfate particles and sand particles with EDX respectively. In the early stage of individual particle analysis, many other researchers have made outstanding achievements (Mamane and Noll, 1985; De Bock et al., 1994; Yamato and Tanaka, 1994; Katrinak et al., 1995;).

In recent years, individual particle analysis became an indispensable methodology. The development of high-resolution micro-electronics has improved the use of this method, with particulate matter identification more accurate. In this review, we summarize the individual particle analysis techniques, including Scanning Electron Microscopy (SEM) coupled with Energy Dispersive X-ray spectrometry (EDX), Transmission Electron Microscopy (TEM) coupled with Energy Dispersive X-ray spectrometry (EDX), Surface-Enhanced Raman Scattering (SERS), Spectroscopy Scanning Transmission X-ray Microscopy (STXM), Scanning Transmission X-ray Microscopy with Near-edge X-ray Absorption Fine-structure (STXM-NEXAFS), Atomic Force Microscopy (AFM), Nanometer-scale Secondary Ion Mass Spectrometry (Nano-SIMS), Time of Flight Secondary Ion Mass Spectrometry (TOF-SIMS), Single Particle Aerosol Mass Spectrometry (SPAMS), Aerosol-Time-Of-Flight Mass Spectrometry (ATOFMS), Ultrafine Aerosol Time-Of-Flight Mass Spectrometer (UF-ATOFMS), and Micro-Raman Spectroscopy (Micro-RS) without SERS. Most of individual particle analysis techniques use high-energy particle beam incident on particle surface and collect physical signals excited by the interaction between high-energy particle beam and particle surface atoms to obtain information about individual particle. These individual particle analysis techniques can provide detailed insights into particle origin, formation, migration, reactions, mixing mechanisms, aging status, and environmental effects, and human health impact.

In this review, the technologies used to analyze individual particles, the type of

individual particles appropriate for these techniques, the sources of individual particles and their characteristics, and the influence and behavior of individual particles (hygroscopicity, optical effects, climatic effects, transport, and health effects) are reviewed.

2 Methodologies of individual particles analysis

There are offline and online techniques in individual particle analyses. Offline methods for the individual particle analysis include SEM-EDX, TEM-EDX, SERS, STXM-NEXAFS, AFM, Nano-SIMS, and TOF-SIMS. Online methods and equipment for individual particle analysis include SPAMS, ATOFMS, UF-ATOFMS and Micro-RS.

SEM-EDX has high resolution (20nm) and is suitable for particles larger than 100nm. SEM-EDX can obtain the three-dimensional morphological characteristics of particles and the element composition on the surface of particles, but only the information on the surface of particles (Li and Shao, 2010).

TEM-EDX has higher resolution (0.1nm) and is suitable for particles smaller than 2μm. TEM-EDX can obtain internal information about particles but operating the TEM-EDX is complex and expensive, and its detection of N is poor (Li et al., 2016b; Xing et al., 2020). Cryogenic TEM and Scanning TEM are also methods under the category of TEM. Cryogenic TEM has advantages in detecting the microstructure of volatile atmospheric particles, excluding the influence of volatile component loss on particle morphology and composition (Li et al., 2021). Scanning TEM mode is more convenient for particle analysis than manual processing, saving a large amount of work and time (Yuan et al., 2021).

SERS is a comprehensive technology for sample detection, that is a good supplement to traditional electron microscopy methods. SERS is very effective in monitoring the mass concentration of sulfate and nitrate. In addition, SERS can observe the evaporative behaviour of sulfate under vacuum conditions, but it cannot provide images and particle size information (Sun et al., 2019).

STXM can study specific bond types in aerosols, as can Nano-SIMS and TOF-SIMS. The resolution of STXM images is 35nm, and the resolution of the energy spectrum is 100nm. STXM is suitable for particles greater than 100nm and can characterize the morphology and functional groups of aerosol particles, but the spatial resolution of STXM is low (Fraund et al., 2019).

AFM can also obtain the three-dimensional morphology of particles, which is suitable for particles smaller than 2μm. AFM can study the surface texture, viscosity, deformation, and elasticity of particles (Shi et al., 2015; Zhang et al., 2020a), but it cannot provide information about the composition of those particles.

Nano-SIMS is suitable for particles larger than 50nm and is sometimes used to study the isotopic characteristics of individual particles, but more often it is used to characterize the mixing state of aerosols, especially the mixing characteristics of organic matter, sulfate, and nitrate (Ghosal et al., 2014; Li et al., 2016a). However, Nano-SIMS is not suitable for statistical analysis because it requires manual operation and statistics and is also very expensive.

TOF-SIMS is suitable for particles larger than 100nm and can obtain the surface chemical composition of aerosol particles, the depth distribution of chemical components, surface, and three-dimensional images (Tervahattu et al., 2002; Lazzeri et al., 2003), but the spatial resolution is low.

SPAMS uses a high-energy pulsed laser as the ionization source, which can analytically ionize almost all kinds of particles. SPAMS is used for particles larger than 100nm, and the main particle size range is 0.2-2.5μm. SPAMS can obtain the chemical composition and size information of particles, but it cannot provide the images of those particles (Chen et al., 2017b; Peng et al., 2020; Shen et al., 2020).

ATOFMS/UF-ATOFMS uses aerodynamic lens focused injection and provides real-time size and chemical composition data of individual particles using a dual laser caliper system and a two-stage Time-Of-Flight Mass Analyzer (Toner et al., 2006). ATOFMS can detect a particle size range of 0.1μm-3μm (Gard et al., 1997). Different versions of ATOFMS can measure different compositions of aerosol particles, such as

organic matter, sulfate, nitrate, metal, and mineral (Middlebrook et al., 2003). UF-ATOFMS instrument incorporated an aerodynamic lens for improving transmission of smaller accumulation mode and ultrafine particles. UF-ATOFMS can provide a particle size range of 50-300nm (Toner et al., 2008), but cannot provide individual particle images.

Micro-RS collects spectral data corresponding to molecules and functional groups under normal ambient conditions and can monitor the changes in morphology and chemical composition of individual particles during their reaction with trace gases. Micro-RS without SERS was also used to detect the chemical composition of individual atmospheric particles (Wang et al., 2021b).

In general, although online individual particle analysis is more convenient and has a higher efficiency in the chemical characterization of pollutants, what is obtained is still the overall chemical compositions of the particulate matters, and the method cannot provide detailed information on the internal structure and the inhomogeneous chemistry. Although the overall chemical compositions of the particulate matter by these online methods are useful in determining the total compositions of particles, the results obtained are more or less similar to those by the bulk analysis methods. In contrast, offline individual particle analysis represented by SEM-EDX and TEM-EDX can be used to observe the detailed morphology, internal structure, phase-separated elemental distribution, mixing states, and all this information can be used to analyze the sources, secondary chemical reaction and even can be extended to the assessment of climatic effects and health effects of particulate matter.

3 Classifications of atmospheric aerosol individual particles

SEM-EDX and TEM-EDX are the two common methods for individual particle analysis. In this review, we mainly consider SEM-EDX and TEM-EDX for the classification of individual particles. Based on EDX analysis and the morphology of individual particles, atmospheric aerosol individual particles are divided into three categories, carbonaceous particles, non-carbonaceous particles, and mixed particles.

Carbonaceous particles include soot particles, organic particles, and biological particles. Non-carbonaceous particles include mineral particles, metal particles, fly ash particles, S-rich (Sulphur-rich) particles, K-rich particles, and sea salt particles (Shi et al., 2003; Yue et al., 2006; Adachi et al., 2010; Adachi and Buseck, 2011; Li et al., 2010b; Li et al., 2020a; Dehghani et al., 2017; Liu et al., 2017; Shao et al., 2017; Hou et al., 2018a; Hu et al., 2018; Abbasi et al., 2019; Wang et al., 2019a; Xing et al., 2020). There are many types of mixed particles, which will be introduced in the following chapters.

3.1 Carbonaceous particles

Soot particles (Fig. 1a), also known as the major types of particles containing black carbon (BC) or elemental carbon (EC), are chain-like aggregates (Fig. 1d) containing spherical carbonaceous particles with sizes ranging from 10 to 100nm (Li et al., 2016b). Soot particles show onion – like structure at high resolution (Fig. 11a$_4$). Soot particles (chain-like, cluster-like, and compact-like) are extremely stable under the electron beam. The soot particles may emission from fossil fuels combustion and biomass burning (China et al., 2013; Xing et al., 2017). The main element of soot particles is C, but they can also contain small amounts of O, Si and K. During the aging process, soot particles can change from chain-like (Fig. 15g) to cluster-like (Fig. 15h), and eventually become compact-like (Fig. 15i) in shape. Some soot particles also formed core-shell structure (Fig. 15j) in shape during the aging process.

Organic particles (Fig. 2) include Primary Organic Matter (POM) and Secondary Organic Matter (SOM); often referred to as OM particles. OM particles also include tar balls. The POM (also known as brown carbon) is spherical or nearly spherical (Fig. 2a, 2d) and extremely stable under the electron beam, and are easily identified under electron microscopy, with diameters ranging from 30nm-500nm (Posfai et al., 2004; Posfai et al., 2013a). Secondary organic particles tend to be irregular in shape (Fig 2b), and often are mixed with secondary sulfate particles. Secondary organic particles can disintegrate rapidly under the electron beam (Hou et al., 2018a). Organic Particles may also form core-shell structure in shape after aging (Fig. 2c). Organic particles are mainly

derived from fossil fuels and biomass combustion (Li and Shao, 2009a; Posfai and Buseck, 2010; Liu et al., 2017; Xing et al., 2019). Organic particles are mainly composed of C and O, and typically contain a small amount of S, Na, Mg, K, and other trace elements.

Biological particles (Fig. 3), also known as bioclasts, generally have specific morphologies and composition, they include spore (Fig. 3a, 3b), bacteria (Fig. 3c), and plant debris (Fig. 3d). Biological particles are mainly composed of C, O, P, K and Si and the size is mainly between 1.8-10μm (Li et al., 2020a).

3.2 Non-carbonaceous particles

Mineral particles (Fig. 4) include long-axis (Fig. 4g), irregular (Fig. 4h) and regular (Fig. 4i) in shape and are very stable under the electron beam. Mineral particles can be either anthropogenic or natural and mainly come from construction dust, road dust and crustal dust. Most mineral particles, often larger than 2μm, originate from the long-distance transport of sandstorm materials or road-suspended dust (Okada et al., 2005；Ramírez et al., 2020). Mineral particles are mainly composed of crustal elements, such as Si, Al, Ca, and Fe (Li and Shao, 2013). The common mineral particles collected in dust storms or dusty atmospheric conditions are mainly feldspar minerals (Fig. 4a), clay minerals (Fig. 4b), carbonate minerals (Fig. 4c), sulfate minerals (Fig. 4d), quartz (Fig. 4e) and unidentified minerals (Fig. 4f). (Wang et al., 2021a).

Metal particles (Fig. 5) are sourced from heavy industry, fuel combustion, vehicle wear, and train track wear (Moreno et al., 2015), and the main elements are Fe (Fig. 5c), Zn (Fig. 5a), and Pb (Fig. 5b) (Liati et al., 2013). They can exist as pure metal or metal oxides. The metal particles are not volatile under the electron beam. Metal particles from combustion-sourced tend to be spherical in shape (Fig. 5c), whereas abrasion-sourced tend to me more angular.

Fly ash particles (Fig. 6a, 6c) are usually spherical in shape and mainly composed of aluminosilicates (Fig. 6b) with occasional small amounts of Ca, Ti, Mn, and Fe. Fly ash particles with small particle sizes easily mix with sulfate to form composite particles

and rarely exist alone. Coal combustion is a common source of fly ash particles (Kashiwakura et al., 2010; Wang et al., 2019a), producing non-crystalline (glassy) particles that can later partially crystallize (Lawson et al., 2020).

S-rich particles (Fig. 7a, 7b, 7c) tend to be irregular in shape and can be volatile under the electron beam, typically forming 'foam-like' structure (Fig. 7a). Some S-rich particles form core-shell structure after aging (Fig. 7b). The composition of shell may be organic, sulfate, nitrate, and other inorganic salts (Wang et al., 2021b). Sulfate particles are the most common S-rich particles in the atmosphere. A study reported that spherical particles dominated the fine mode in urban and marine samples, these particles were droplets containing ammonium sulfate (Zhang et al., 2000).

K-rich particles (Fig. 8) are a commonly used marker for biomass combustion although coal combustion also contains a small amount of K (Lu et al., 2017; Zhang et al., 2020a). K-rich particles in the atmosphere are mainly composed of K, N, Cl and S usually with irregular shapes (Fig. 8b) (Bi et al., 2011; Giordano et al., 2015). When the main elements of K-rich particles are K and Cl and have a crystalline structure, they are usually KCl particles (Fig. 8a). Changes in the elemental ratios of Cl/Na and S/Na in sea-salt particles are expected from the atmospheric reactions of sulfuric and nitric acids with these particles (McInnes et al., 1994).

Sea salt particles (Fig. 9) are mainly sourced from the ocean or evaporated lakes, and the main elements are Na, Cl and S (Frey et al., 2020). Sea salt particles are stable under the electron beam and are typically seen with cubic NaCl crystalline morphology (Fig. 9a, 9b). In certain particle collection devices, the NaCl can dissolve then recrystallize on the collection substrates (Jones et al., 2001). In some humid coastal environments, the cubic sea salt crystals tend to form amorphous sea salt particles after aging (Fig. 9c) (Li et al., 2010a).

3.3 Mixed particles

Particles in the atmosphere often does not exist as a single phase of chemical composition. For example, due to the high humidity in haze weather, the physical and

chemical reaction between particles is more intense than that in non-haze days. Under these conditions, particles tend to appear in a mixed state (Fig. 10). The mixing state of particles affects their physical and chemical properties (Zhang et al., 2008), so it is necessary to understand the make-up of individual mixed particles. Individual particle analysis has many advantages in the study of these mixed particles, compared to bulk analysis. The mixing state of individual particle can be divided into internal mixing and external mixing. External mixing is defined as no contact between particles and no change in the physical and chemical properties between particles. Internal mixing is defined as the simultaneous presence of two or more aerosol components in an individual particle (Li et al., 2016c). The term "mixed particles" used in this review refers to the internal mixed particles. We divide the internal mixing into heterogeneous mixing and inhomogeneous mixing. Homogeneous mixing refers to the uniformity of mixing between particles, indicating a total mixing. Heterogeneous mixing often shows a mixture of multiple phases of particles, indicating an incomplete mixing. Based on the morphology and internal structure, the internal mixed particles can be subdivided into two structural types, that is, irregular mixing shape (Fig. 10a, 10b) and core-shell structure (Fig. 10d). In terms of chemical compositions, the internal mixed particles have been divided into the organic and sulfate mixed particles (Fig. 10a), organic and soot mixed particles (Fig. 10b), organic and K-rich mixed particles (Fig. 10c), S-rich and fly ash mixed particles (Fig. 10d), S-rich and metal mixed particles (Fig. 10e), S-rich and mineral mixed particles (Fig. 10f), S-rich and soot mixed particles (Fig. 10g) and K-rich and metal mixed particle (Fig. 10h) (Table 3) (Fan et al., 2016a; Li et al., 2016c; Chen et al., 2017a; Zhang et al., 2017; Hou et al., 2018a; Liu et al., 2018; Yu et al., 2019; Zhang et al., 2018).

4 Source analysis of different types of individual particles

The aim of source apportionment of atmospheric particulate matter is to identify, either qualitatively or quantitatively, the sources of atmospheric particulate matter to environmental receptors using chemical, physical, mathematical, or other methods. The

results of source apportionment can not only identify the outcomes of differentiated management and control of key areas and sources at the local level, but also help to develop fast, scientific, effective, and feasible solutions. When the elemental mixtures in the particulate matter are complex, traditional bulk analytical methods ignore low concentrations of toxic and characteristic elements, resulting in errors in the results. Individual particle analysis can directly observe and characterize properties of individual particles in relation to their sources, which potentially can provide high resolution of source apportionment and avoid artifacts or confounding factors.

The individual particle analysis observes the morphological characteristics of individual particles by electron microscopy and the characteristic compositional spectra observed by EDX, and by these criteria, the possible sources of individual particles can be classified. According to the Technical Guide for the Source Analysis of Particulate Matter in the Atmosphere, particulate matter emission sources can be divided into stationary combustion sources, biomass open combustion sources, industrial process sources and mobile sources. Among them, the stationary combustion sources include power generation, industrial, and domestic use (coal, diesel, oil, kerosene, fuel oil, liquefied petroleum gas, gas, natural gas, and other fuel types). Industrial process sources include metallurgy, building materials, chemical and many other industries. In the process of source analysis, the bench experiments are the most direct method to trace the source of atmospheric particles, and smog chamber experiments are the most direct method to detect the formation of new particles and atmospheric heterogeneous reactions.

4.1 Fingerprint features of individual aerosol particles

Microscopy is a method that allows the probable determination of the source of particulate matter from the microscopic information of individual particles. Microscopy is therefore suitable for the analysis of particulates with obvious morphological characteristics. Individual particle analysis can obtain the type, size, quantity, shape, color, optical properties, chemical composition, and other characteristics of particles.

Individual particle analysis can also be used to visually identify the most likely source of particulate matter. The bench experiment is to analyze the particles emitted from the source sample and directly characterize the source of the particles. The results for coal burning, biomass burning, and vehicle exhaust sources can provide information on the primary particles in the atmosphere.

4.1.1 Coal burning bench experiments

Emissions from coal burning is an important source of gaseous and particulate pollutants in the atmosphere, with fine particles emitted being one of the main causes of regional haze in China (Jones et al., 2009; Pui et al., 2014). After the State Council of China issued the "Air Pollution Prevention and Control Action Plan" (APPCAP) on September 10, 2013 (The State Council of China, 2013), the energy infrastructure changed with a dramatic decrease in coal consumption; however, domestic coal burning still contributes a significant amount of $PM_{2.5}$ to the atmosphere due to incomplete combustion and dedust devices (Li et al., 2016c; Li et al., 2020b). Wang et al (2019a) used a measurement system of an atmospheric dilution chamber in the laboratory to show that the particulate matter produced by coal combustion mainly includes S-rich particles (Fig. 11a_1), mineral particles (Fig. 11a_2), soot particles (Fig. 11a_3) and organic particles (Fig. 11a_5). In the ignition stage, organic particles accounted for the largest proportion, up to 66%. In the intense combustion stage, soot particles accounted for the largest proportion, up to 71%, In the final charcoal burning stage, mineral particles accounted for the largest proportion, up to 73% (Wang et al., 2019a). Hou et al. (2018b) also showed that the particles produced by coal burning can be divided into soot particles, organic particles, mineral particles, sulfate, and metal particles. Related studies have found that in the combustion of low rank coal the particles emitted are mainly carbonaceous particles (organic particles and soot particles), while the particles emitted from high rank coal burning are mainly organic and sulfate mixed particles (Zhang et al., 2018). Therefore, in the different combustion stages and temperatures the characteristics of particles are different, also the coal rank will result in different types

of particles being emitted.

4.1.2 Biomass burning bench experiments

Agricultural waste is volumetrically one of the most burned biomasses in the world. The open burning of agricultural residues is a convenient and inexpensive way to prepare for the next crop but can lead to serious regional haze events (Tariq et al., 2016). Biomass combustion emits large numbers of organic particles and gaseous pollutants, including Non-Methane Volatile Organic Compounds (NMVOCs), CO, CO_2, CH_4, NO_x, NH_3, OC, EC and metals (Bond et al., 2004; Li et al., 2007; Chang-Graham et al., 2011; Heringa et al., 2011; Bond et al., 2013; Laskin et al., 2015). Biomass burning is also the second largest source of non-methane organic gases in the atmosphere (Stockwell et al., 2014). Li et al. (2021b) showed that there were mainly five types of particles in straw burning of corn, wheat and rice. These were soot particles (Fig. 11b_1), K-rich particles (Fig. 11b_2), tar balls (Fig. 11b_3), organic containing K particles (Fig. 11b_4) and pure organic particles respectively (Fig. 11b_5). Organic containing K particles accounted for the most, followed by organic particles. Soot particles only appear in the flaming burning stage (Li, 2021). When comparing the particles emitted by coal burning, it is found that soot particles are greatly reduced, and there are very few S-rich particles and mineral particles emitted by biomass burning.

4.1.3 Vehicle exhaust emissions bench experiments

Vehicle exhaust emissions are major sources of airborne particles in the urban atmosphere (Hwa and Yu, 2014). The secondary aerosol formed by the particles from motor vehicle exhaust is an important component in the formation of haze (Huang et al., 2014). Studies have shown that the number of particle emissions of gasoline engines are usually lower than those from diesel engines (Alves et al., 2015). Xing et al. (2020) found that GDI (gasoline-direct-injection) engine and PFI (port fuel injection) engine mainly emitted six types of particles. they were soot particles (Fig. 11c_1), Ca-rich particles (Fig. 11c_2), organic particles (Fig. 11c_3), S-rich particles (Fig. 11c_4), Fe-rich

(Fig. 11c_5) and other particles. Soot particles accounted for the highest proportion of those emitted by GDI engine, and organic particles accounted for the highest proportion by PFI engine (Fig. 12) (Xing, 2018). Xing et al. (2020) also found that when gasoline direct-injection engines are in a cold start and acceleration conditions, soot particles accounted for a greater proportion (Xing et al., 2020).

4.2 The formation of secondary particles and heterogeneous reactions

Airborne particles can be thought of as suspensions in reaction containers in which there are numerous chemical and physical processes, such as multiple phase reactions and gas-particle distributions (Poschl, 2005; Kuwata and Martin, 2012). The heterogeneous reactions between aerosol particles and trace gases can change the mixing state of aerosol particles and the composition of those particles, through several physical and chemical processes (Fuzzi et al., 2006; Zhang et al., 2008; Posfai and Buseck, 2010). Li et al. (2011) showed that secondary nitrate and sulfate mixed with soot and sea salt particles could completely change the surface moisture absorption properties. Recent studies have shown that liquid particles can accelerate the mass transfer and multiphase reaction of reactive trace gases, promote the formation of secondary aerosols, and eventually lead to the rapid increase of aerosol mass (Liu et al., 2019).

Core-shell structure was considered as a sign of particle aging (Niu et al., 2011, 2012). The surface of the core can be used as a heterogeneous reaction site for SO_2 and NO_x (Ebert et al., 2016). The ratio of core to shell is usually used to measure the degree of particle aging. The smaller the ratio is, the more aging the particle. Sometimes the coating thickness of core-shell structure particles can also be used to directly estimate the degree of particle aging. The greater the coating thickness is, the more aging the particle. Xu et al. (2019) showed that organic particles with larger particle sizes had a higher degree of aging than those with smaller particle sizes, and S-rich particles along the coast showed more indications of aging than those collected in their urban site (Xu et al., 2019). Hou et al. (2018) showed that the particles in the city are aged than those

collected in a local highway tunnel, which was due to the higher solar radiation in the city. Under solar radiation, photochemical reactions can promote the aging of primary particles to form large numbers of secondary organic aerosols (Miracolo et al., 2011). The mixing state and aging process of particulate matter play an important role in atmospheric circulation, which will have an important impact on the future study of aerosol impacts on regional and global climate. Smog chamber experiments are an important method to study the heterogeneous reaction and aging of atmospheric particles. Details of chamber setups and associated facilities can be found in Deng et al., (2017) and Liu et al., (2015).

4.2.1 Smog chamber experiments; coal burning particles

Coal burning emitted large amounts of particles (organic particles, soot particles, sulfate particles and mineral particles), which is a major source of regional air pollutant $PM_{2.5}$. In addition, coal burning also emits gaseous pollutants such as VOCs, NOx and SO_2. These solid and gaseous pollutants can participate in physical and chemical processes in the atmospheric environment, such as nucleation, condensation, gas/particle collision, heterogeneous reaction, or multiphase reaction, and form secondary organic aerosols (SOA). Jaoui et al. (2012) found that SO_2 can promote the generation of anthropogenic and biological VOCs for SOA, and showed that heterogeneous reaction is an important way for the transformation of organic compounds from gas phase to granular phase. The smoke chamber experiments shows that large numbers of secondary particulate matter are generated in the photochemical reaction of the flue gas emitted from coal burning. The morphology of soot particles changed from chain (Fig. 13a) to cluster dense structure (Fig. 13b). The morphology of organic particles changed from spherical or quasi-spherical (Fig. 13c) to irregular shape (Fig. 13d, 2c). Some fresh S-rich particles (Fig. 13e) formed core-shell structure in shape (Fig. 13f) (Li, 2021).

506 4.2.2 Smog chamber experiments; biomass burning particles

507 Aerosol particles emitted by biomass burning have a significant impact on regional
508 and global atmospheric environment and climate, especially in developing countries,
509 where crop straw burning emissions aggravate air pollution. Primary particles emitted
510 from biomass combustion will age in the air, which directly leads to the formation of
511 secondary particles, thus exacerbating the formation of regional haze. Li et al. (2003)
512 found that K-rich particles in aerosol emitted by biomass burning would be converted
513 into K_2SO_4 and KNO_3 in the photochemical reaction. Hennigan et al. (2011) found that
514 the emission of organic particles from wood burning increased due to photochemical
515 oxidation reaction. The smog chamber simulation experiment found that the micro
516 morphology and chemical composition of particles changed after primary particles
517 aging. It mainly shows that the K-rich particles change from the initial crystal
518 morphology (Fig. 14a) to the irregular shape of inclusions (Fig. 14c); In terms of
519 elements, the content of S increased in particles. K-rich particles are mainly KCl
520 particles in the early stage and are gradually vulcanized in the aging process to form
521 more K_2SO_4 particles. The aging process of soot particles also observed that during the
522 aging process, soot particles changed from chain-like (Fig. 14d) to cluster-like (Fig.
523 15e), and become compact-like (Fig. 15f) in shape (Li, 2021).

524 4.2.3 Smog chamber experiments; vehicle exhaust emission particles

525 Vehicle exhausts emit a large amount of primary particulate matter, which is an
526 important source of $PM_{2.5}$ in the atmosphere. However, gaseous pollutants such as SO_2,
527 NO_X and VOCs emitted by motor vehicle exhaust can generate secondary particulate
528 matter through physical and chemical reactions in the atmospheric environment, and
529 their contribution to $PM_{2.5}$ can also not be ignored. The smog chamber experiments
530 shows that in Beijing urban atmosphere, gasoline vehicle exhaust rapidly (only 3.5
531 hours) formed large numbers of secondary organic particles, and the primary particles
532 also aged. The generation of secondary particles and the aging of primary particles are
533 affected by a variety of factors, among which the more important are the initial

concentration of pollutants discharged by gasoline vehicles (including VOCS, NO_X, etc.), relative humidity, light intensity, oxidizer (oxidation level) (Ding et al., 2011; Donahue et al., 2012). The smoke chamber experiment shows that large numbers of sulfate particles are generated in the photochemical reaction of the flue gas emitted from vehicle exhaust. The morphology and composition of primary particles emitted from gasoline vehicles changed after aging (Fig. 15a, 15b, 15c). Soot particles changed from chain-like (Fig. 15g) to cluster-like (Fig. 15h), and eventually become compact-like (Fig. 15i) in shape. Some soot particles also change into core-shell structure. The morphology of organic particles and Ca-rich particles changed from a spherical structure (Fig. 15d) to a more irregular shape. In terms of elemental composition, the amount of S element in organic particles and Ca-rich particles increased (Fig. 15f) (Xing, 2018).

5 Applications in the study of climatic change, geochemical cycling, and the human health effects

Individual particle analysis technique is widely used as an important method in characterization of the physical and chemical properties of airborne particles in recent research. Individual particle analysis can detect particle sources, heterogeneous reactions, climatic effects, global geochemical cycling effects, and health effects. The results obtained by individual particle analysis have greatly improved public awareness of the hazards of particles in the atmosphere.

5.1 Airborne particles and climatic change

Airborne particles can directly or indirectly affect the climate. Lage numbers of anthropogenic sources (such as soot, organic and sulfate particles) and natural sources (such as dust and sea salt particles) emitted into the atmosphere will absorb and scatter the incident solar radiation, thus directly changing the energy budget of the Earth-atmosphere system, and ultimately affecting climate change (Fig. 16) (Wang et al., 2018; Adam et al., 2021; Mu et al., 2021). In addition, atmospheric particles can also

act as Cloud Condensation Nuclei (CCN) to change the cloud optical properties and lifetime, and indirectly affect the climate (Buseck and Posfai, 1999; Wang et al., 2019b). Atmospheric particles can also participate in the heterogeneous reaction of ozone to affect ozone balance and indirectly affect the energy budget of the Earth-atmosphere system (McNeill, 2017). The radiation effect of atmospheric particles depends on particle size, spectral distribution, chemical composition, surface characteristics and the relative humidity of the environment (Penner et al., 1992; Fan et al., 2016b; Zieger et al., 2017). In addition, the mixing state of particulate matter (Fig. 17) has also an important impact on climate (Hou, 2017; Wang et al., 2017). When the relative humidity of the surrounding environment increases, atmospheric particles can display hygroscopic behavior, which has an important influence on cloud condensation activity and atmospheric visibility, and can indirectly affect regional or global climate change (Chen et al., 2012a; Lei et al., 2014).

Remote areas at high altitudes are often seen as pristine environments that are particularly sensitive to climate change and have received much attention from scientists. Recent research showed that primary brown carbon particles from biomass burning in South Asia can travel long distances to the high-altitude Himalayas, contributing significantly to local atmospheric warming and potentially affecting glacier melting (Yuan et al., 2020). The study of Zhao et al. (2017) on the Tibet Plateau showed that the direct surface radiative forcing of black carbon (-36.0 Wm^{-2}) is much stronger than the typical levels found at lower altitudes and the contribution of black carbon to the radiative forcing is higher than at lower altitudes.

5.1.1 Indirect climatic effects and the hygroscopicity of particles

When the relative humidity of the atmospheric environment increases, the ability of atmospheric particles to absorb water is called the hygroscopicity of particles (Gasparini et al., 2004). The hygroscopic tandem differential mobility analyzer is the most common method to measure the hygroscopic growth of particles under different modes (Liu and Zhang, 2010). The hygroscopic behavior of atmospheric particles has

a direct or indirect influence on their moisture content, scattering extinction characteristics, heterogeneous reactions on the particle's surface, cloud condensation nucleation characteristics, and human health (Chen et al., 2012a; Lei et al., 2014; Chen et al., 2016). The hygroscopicity of particles will increase the particle size and lead to the increase of the extinction efficiency factor, which makes up for the effect of the reduced surface concentration of particles on the reduced visibility (Yang et al., 2018). The hygroscopicity of atmospheric particles can be expressed by hygroscopicity growth factor $HGF=D_{RH}/D_d$. In this formula, D_{RH} and D_d are the particle size of hygroscopic and dry particles at a certain relative humidity (Wu et al., 2017). Based on Kohler's theory, Petters and Kreidenweis (2007) proposed an individual parameter κ (Kappa), which is independent of relative humidity and particle size, to characterize the hygroscopicity of particles. The study found that the κ value of rural particle collections was higher than that of urban collections (the κ value of urban sites was around 0.1-0.3, the rural sites was about 0.15-0.4) (Wang et al., 2017). Cheung et al. (2020) found that the κ value of cloud condensation nuclei decreased in the early stages of new particle formation and increased in the later stages of new particle formation. Recent research shows that when the relative humidity is 90%, the mass ratios of adsorbed water to dry mineral ranged from 0.0011-0.3080, the hygroscopicity of mineral aerosols depends largely on the BET surface area of mineral aerosols; the method uses a measurement of the physisorption of a gas to derive a value of 'surface area' for a sample (Chen et al., 2020a). In addition, organic matter coating the surface of inorganic salts in the atmosphere usually inhibits deliquiating and hygroscopic growth of inorganic aerosols. Zhang et al. (2020b) showed that the coating of organic shells would lag the deliquiating point of sodium chloride crystals, with the thicker the organic coating, the more obvious the hysteresis effect (hysteresis is the dependence of the state of a system on its history).

The organic particles will be oxidized during aging processes, which will increase the hydrophilic functional groups on the surface of the particles and increase the hygroscopicity and cloud condensation nuclear activity of the particles (Bougiatioti et al., 2016; Slade et al., 2017). Smog chamber simulation experiments show that SO_2 in

618 the atmosphere can promote the formation of some organic aerosols and increase the
619 activity of cloud condensation nuclei (Li et al., 2015). Sea salt particles are an important
620 component of atmospheric particles in coastal cities. Due to the rapid aging of sea salt
621 particles in the urban environment, it has an important influence on hygroscopicity and
622 light scattering (Adachi and Buseck, 2015). Sea salt particles mainly increase the
623 amount of CCN, thus increasing precipitation. However, for mineral particles, due to
624 their high heterogeneity, it is difficult to estimate the effect of atmospheric radiative
625 forcing. Mineral particles can provide an important interface for atmospheric chemical
626 reactions. Mineral particles play an important role in climate effect because of their
627 hygroscopic influence on water circulation in the atmosphere and cloud radiation.
628 Soluble cations (Ca^{2+}, Mg^{2+}, Na^{+} and K^{+}) on the surface of mineral particles can have
629 heterogeneous reactions with atmospheric acids such as HNO_3 or HCl. Meanwhile, the
630 surface of mineral particles can provide a site for the oxidation of SO_2 to H_2SO_4, all
631 these processes will increase the water absorption of mineral particles and eventually
632 form CCN (Karydis et al., 2017). On the other hand, when larger mineral particles form
633 CCN, they will compete with smaller particles for moisture in the air, which will reduce
634 supersaturation and cloud droplet formation (Betancourt and Nenes, 2014). Some
635 mineral particles, such as $CaCO_3$, have low water absorption capacity, but when they
636 form $Ca(NO_3)_2$ or $CaCl_2$ after aging-related reactions in the air, their hygroscopic
637 capacity increases, and the activity of CCN increases (Tang et al., 2015). The
638 hygroscopic properties of atmospheric particles contribute to the study of global or
639 regional climate change.

640 5.1.2 Direct climate effects and atmospheric visibility

641 Particulate matter can cause local and regional environmental deterioration and
642 adversely affect the lives of people, the most visual of which is the impact on visibility.
643 The ‘extinction effect’ caused by absorption and scattering of light by atmospheric
644 particles, especially fine particles, is the main cause of visibility reduction (Tsai, 2005;
645 Wu et al., 2018; Han et al., 2020; Sun et al., 2020). The light absorption effect of

particulate matter is mainly due to black carbon or substances containing black carbon. The extinction effect of EC was 73.5% in atmospheric particles in the winter in Tianjin (Xiao et al., 2014). Studies showed that the aerosol absorption in the winter (395 mm^{-1} at 370 nm and 99 mm^{-1} at 880 nm, respectively) was about 5-8 times that in the autumn (49mm^{-1} at 370nm and 18 mm^{-1} at 880 nm, respectively); at all wavelengths (370nm-950nm), black carbon is the major light-absorbing carbonaceous component (Zhu et al., 2021). Although most organic aerosol components are known to have a cooling effect on the global climate, the brown carbon in organic aerosols can absorb shorter wavelengths of solar radiation and contribute to climate warming (Alexander et al., 2008). Sulphate particles have ability to force negative light radiation and reduce temperature (Liu et al., 2009). The optical properties of atmospheric particles contribute to the study of global or regional climate change.

5.2 Airborne particles and global geochemical cycling

The mobility and high efficiency of the instruments used in individual particle analysis are a great advantage when collecting samples in remote areas, with the potential to better identify the global effects of those particles. Atmospheric particles emitted from urban cities or industrial areas can reach rural areas, remote areas, oceans and even the Arctic (Fig. 19) due to the capacity of the atmosphere to transport them over long distances (Jane and Amber 2015). After dry sedimentation or wet sedimentation, atmospheric particles will participate in biogeochemical cycle (Mahowald et al., 2018; Luo et al., 2019). It is known that large amounts of mineral particles are carried into the atmosphere by strong ground winds and transported over long distances (Adachi et al., 2020; Ono et al., 2020). Long-distance transport of mineral particles can alter biogeochemical processes on land and in the ocean. Li et al. (2014) found that pollutants from haze and Asian dust storms can be transported continental distances. These particles connect the land, atmosphere, and ocean, affecting regional climate and hydrological and biogeochemical cycles. Many studies have shown that long-distance dust storms are preserved in ice cores, ocean floor

sediments, and peat (Lambert et al., 2008; Le Roux et al., 2012). Large amounts of anthropogenic particles are now found in areas where there is little human activity. For example, long-distance transport of light-absorbing carbonaceous aerosols from south Asia was observed in the snow cover of Himalayan glaciers (Dong et al., 2018). Sea salt and sulfate particles coated in organic matter have been found in the Arctic (Yu et al., 2019). Zhao et al. (2019) found that organic matter in Mount Tai (a mountain located north of the city of Tai'an, and the highest point in Shandong province, China) was mixed with regional anthropogenic organic matter and biological organic matter from long-distance atmospheric transport. Analyses of aerosol particles in the Amazon Basin show differences in the fraction of particles transported over long distances and from local sources (Adachi et al., 2020). In the process of long-distance transmission, the acidic gases in the atmosphere, such as SO_2 and NO_2, are absorbed by the particle surface due to heterogeneous reaction with the dust particles, and some particles form a shell structure on the surface and settle on the terrestrial surface (Li and Shao, 2009b).

Dissolution of particulate matter transported over long distances has significant effects on water, soil, plants, biological communities, and climate. Bioaerosol transport may affect ocean-atmosphere interactions (Yue et al., 2019). Fe particle emissions from fossil fuels may be transported to remote areas of the ocean and affect the primary productivity of phytoplankton and the carbon cycle (Pinedo-Gonzalez et al., 2020). Large numbers of pollutants such as SO_2 discharged into the atmosphere increased the content of soluble Fe in the air, which was transported to the marine environment over a long distance, thus increasing the amount of Fe available to marine organisms and changing biological activities (Li et al., 2017). Zhang et al. (2019) found that N increased carbon fixation and indirectly offset global warming. Hg adsorbed on particles can be transported horizontally (long distances) or vertically (deposition) or incorporated into nutrient chains and transmitted to organisms via food, making important contributions to root uptake, leaf deposition, and leaf absorption metal accumulation in plants (Beldowska et al., 2018). Because black carbon particles stay in the free troposphere for a long time, black carbon particles can be transported from the

703 tropical low troposphere for a long distance and have an impact on the climate in the
704 far southern hemisphere (Wiedensohler et al., 2018). Research showed that the east
705 coast of the United States is affected by long-distance particle transport from various
706 sources throughout the year, which affects the local precipitation rates (Aldhaif et al.,
707 2020). The global geochemical cycling of individual particles provides important
708 information for regional haze control, climate effect and health risk assessment

709 5.3 Airborne particles and human health effects

710 Long-term exposure to atmospheric pollution increases the risk of diseases of the
711 respiratory and cardiovascular systems (Fig. 20). According to statistics in 2015,
712 globally 8.8 million people died due to atmospheric pollution, and the average life
713 expectancy of humans was reduced by 2.9 years (Lelieveld et al., 2020). There was a
714 significant correlation between PM_{10} mass concentration and mortality, especially from
715 cardiovascular and respiratory diseases (Cao et al., 2012; Chen et al., 2012b). The
716 atmosphere contains a variety of toxic and harmful substances, including polycyclic
717 aromatic hydrocarbons and their derivatives, heavy metals (Zn, Cu, Cd, Cr, Pb, Mn, Tl,
718 etc.), black carbon particles, asbestos fibers, and radioactive substances. Short term
719 atmospheric pollution exposure can lead to lung inflammation or lung damage, and
720 long-term exposure can lead to chronic obstructive pulmonary disease, or even lung
721 cancer (Xue et al., 2019; Chen et al., 2020b).

722 The degree of harm from atmospheric particles to human health mainly depends
723 on the particle size, number, and composition (Dockery and Pope, 1994). The smaller
724 the particle size, the larger the surface area, onto which harmful substances, viruses and
725 bacteria can be adsorbed (Georgakakou et al., 2016). The composition of the particles
726 is one of the main pathogenic factors and determines the type of disease. The
727 concentration of particles and the exposure time determine the inhaled dose by the
728 human body. The higher the particle concentration, the longer the exposure time, the
729 greater the harm to the human body. A variety of individual particle types, such as
730 nanoscale soot particles (Fig. 18c), organic particles (Fig. 2) and metal particles (Fig.

5), are all toxic components of $PM_{2.5}$ (Dockery and Pope, 1994; Shao et al., 2006a). Shao et al. (2007) compared the DNA damage caused by soot particles, mineral particles, fly ash particles and unknown fine particles, and found that soot and unknown fine particles were important components leading to a raised plasmid DNA damage. TEM analysis demonstrated that the toxic metal particles rich in Fe, Zn, Pb and Mn are usually nanometer in size and abundant in the atmosphere (Li et al., 2013a). Studies have shown that the mixing of particles (Fig. 18) can also convert insoluble metal oxides into metal ions (Fig. 4b) that can be deposited in the body (Baltrusaitis et al., 2012). Nano-sized metal particles of Cu in the air may affect neurological diseases, and soluble Zn in airborne particles can damage lung cells (Richards et al., 1989; Richards, 2003; Manigrasso et al., 2019). Studies have shown that combined exposure to Fe and black carbon particles induces oxidative damage, cytotoxicity, and pro-inflammatory responses in the lung (Zhong et al., 2010). Long-term exposure to black carbon may also lead to increased eye pressure (Manigrasso et al., 2019). The toxicological properties of atmospheric particles have improved the public's awareness of the risks presented by atmospheric haze.

6 Future research on individual particle analysis; prospects and priorities

Individual particle analysis technology has been used in various research fields of atmospheric environmental science, showing a huge potential. Individual particle analysis technology has obtained some exciting research results and opened a new field for the study of atmospheric environmental science. However, the potential of individual particle analysis has not been fully exploited, and the application of individual particle analysis in atmospheric environment science is not systematic.

Future research is likely to include the following aspects.

1) The optimization of individual particle methodologies and instruments is always an urgent task, which would allow more advanced and accurate results. This will enable research on the physical and chemical properties, optical properties, and environmental effects of atmospheric particulate matter. It will

759 be important to standardize manual and automatic methods.
760 2) Obtaining large and scientifically vigorous database of individual particle
761 analysis statistics is critical, including image processing. Currently individual
762 particle statistical analysis and image processing is very time-consuming
763 research. It would significantly benefit from improved computer software and
764 big data idea for automated particle data processing, generating more reliable
765 statistics and processed imagery.
766 3) Further study is required on individual particle source apportionment, especially
767 with the optimization of electron microscopes to analyze more particles in a
768 more practical way. This should include establishing more accurate source
769 apportionment models, refining, and improving dynamic emission inventories,
770 and improving emission information from key industries. In addition, there is a
771 critical need to identify sensitive sources that have significant effects on human
772 health, atmospheric environment, and effective controls.
773 4) The role of atmospheric particulate matter on climate is an important issue and
774 special attention should be paid on the influence and relationship between
775 particulate matter and a rapidly changing global climate. Key aspects of this
776 would include: studying the scattering and absorption effects of different
777 particle types; exploring the effects of particles on solar radiation and the global
778 heat balance; elucidating the hygroscopicity and heterogeneous reactions of
779 different types of atmospheric particles; evaluating the process of cloud
780 condensation nuclei of different particle types. The importance of individual
781 particle analysis in climate research should be promoted.
782 5) It must be understood that this research is interdisciplinary, integrating with
783 natural science disciplines such as mathematics, physics, chemistry, earth
784 science, life science and information science. The use of ‘big data’
785 methodologies is now commonplace, and presents opportunities to
786 comprehensively study the atmosphere, particulate matter, meteorology, climate,
787 and health.
788

Acknowledgments

This study is supported by the National Natural Science Foundation of China (Grant No. 42075107, 41175109), the Projects of International Cooperation and Exchanges NSFC (Grant No. 41571130031), the Fundamental Research Funds for the Central Universities, and the Yueqi Scholar fund of China University of Mining and Technology (Beijing).

References

Abbasi, S., Keshavarzi, B., Moore, F., Turner, A., Kelly, F.J., Dominguez, A.O., Jaafarzadeh, N., 2019. Distribution and potential health impacts of microplastics and microrubbers in air and street dusts from Asaluyeh County, Iran. Environ Pollut. 244, 153-164.

Adachi, K., Buseck, P.R., 2011. Atmospheric tar balls from biomass burning in Mexico. J Geophys Res-Atmos. 116, D05204.

Adachi, K., Buseck, P.R., 2015. Changes in shape and composition of sea salt particles upon aging in an urban atmosphere. Atmos Environ. 100, 1-9.

Adachi, K., Chung, S.H., Buseck, P.R., 2010. Shapes of soot aerosol particles and implications for their effects on climate. J Geophys Res-Atmos. 115, D15206.

Adachi, K., Oshima, N., Gong, Z., de Sa, S., Bateman, A.P., Martin, S.T., de Brito, J.F., Artaxo, P., Cirino, G.G., Sedlacek, A.J., III, Buseck, P.R., 2020. Mixing states of Amazon basin aerosol particles transported over long distances using transmission electron microscopy. Atmos Chem Phys. 20, 11923-11939.

Adam, M.G., Tran, P.T.M., Bolan, N., Balasubramanian, R., 2021. Biomass burning-derived airborne particulate matter in Southeast Asia: A critical review. J Hazard Mater. 407, 124760.

Aldhaif, A.M., Lopez, D.H., Dadashazar, H., Sorooshian, A., 2020. Sources, frequency, and chemical nature of dust events impacting the United States East coast. Atmos Environ. 231, 117456.

Alexander, D.T.L., Crozier, P.A., Anderson, J.R., 2008. Brown carbon spheres in East Asian outflow and their optical properties. Science. 321, 833-836.

Alves, C.A., Lopes, D.J., Calvo, A.I., Evtyugina, M., Rocha, S., Nunes, T., 2015. Emissions from light duty diesel and gasoline in use vehicles measured on chassis dynamometer test cycles. Aerosol Air Qual Res. 15, 99-116.

Ari, A., Ari, P.E., Gaga, E.O., 2020. Chemical characterization of size segregated particulate matter by inductively coupled plasma- Tandem mass spectrometry. Talanta. 208, 120350.

825 Ayash, T., Gong, S., Jia, C.Q., 2008. Direct and indirect shortwave radiative effects
826 of sea salt aerosols. J Climate. 21, 3207-3220.
827 Ayers, G.P., 1977. An improved thin film sulphate test for submicro particles.
828 Atoms Environ. 11, 391-395.
829 Baltrusaitis, J., Chen, H., Rubasinghege, G., Grassian, V.H., 2012. Heterogeneous
830 atmospheric chemistry of lead oxide particles with nitrogen dioxide increases lead
831 solubility: environmental and health implications. Environ Sci Technol. 46, 12806-
832 12813.
833 Beldowska, M., Saniewska, D., Gebka, K., Kwasigroch, U., Korejwo, E., Kobos,
834 J., 2018. Simple screening technique for determination of adsorbed and absorbed
835 mercury in particulate matter in atmospheric and aquatic environment. Talanta. 182,
836 340-347.
837 Betancourt, R.M., Nenes, A., 2014. Droplet activation parameterization: the
838 population splitting concept revisited. Geosci Model Dev. 7, 2345-2357.
839 Bi, X., Zhang, G., Li, L., Wang, X., Li, M., Sheng, G., Fu, J., Zhou, Z., 2011.
840 Mixing state of biomass burning particles by single particle aerosol mass spectrometer
841 in the urban area of PRD, China. Atmos Environ. 45, 3447-3453.
842 Bigg, E.K., Ono, A., Williams, j.A., 1974. Chemaical tests for individual
843 submicron aerosol particles. Atmos Environ. 8, 1-13.
844 Bond, T.C., Doherty, S.J., Fahey, D.W., Forster, P.M., Berntsen, T., DeAngelo, B.J.,
845 Flanner, M.G., Ghan, S., Kaercher, B., Koch, D., Kinne, S., Kondo, Y., Quinn, P.K.,
846 Sarofim, M.C., Schultz, M.G., Schulz, M., Venkataraman, C., Zhang, H., Zhang, S.,
847 Bellouin, N., Guttikunda, S.K., Hopke, P.K., Jacobson, M.Z., Kaiser, J.W., Klimont, Z.,
848 Lohmann, U., Schwarz, J.P., Shindell, D., Storelvmo, T., Warren, S.G., Zender, C.S.,
849 2013. Bounding the role of black carbon in the climate system: A scientific assessment.
850 J Geophys Res-Atmos. 118, 5380-5552.
851 Bond, T.C., Streets, D.G., Yarber, K.F., Nelson, S.M., Woo, J.H., Klimont, Z., 2004.
852 A technology-based global inventory of black and organic carbon emissions from
853 combustion. J Geophys Res-Atmos. 109, D14203.

Bougiatioti, A., Bezantakos, S., Stavroulas, I., Kalivitis, N., Kokkalis, P., Biskos, G., Mihalopoulos, N., Papayannis, A., Nenes, A., 2016. Biomass-burning impact on CCN number, hygroscopicity and cloud formation during summertime in the eastern Mediterranean. Atmos Chem Phys. 16, 7389-7409.

Buiarelli, F., Di Filippo, P., Pomata, D., Riccardi, C., Simonetti, G., 2018. A rapid method for the determination of levoglucosan in NIST standard reference material 1649a by HPLC-MS/MS. Atmos Environ. 195, 24-29.

Buseck, P.R., Posfai, M., 1999. Airborne minerals and related aerosol particles: Effects on climate and the environment. P Natl Acad Sci USA. 96, 3372-3379.

Cao, C., Jiang, W., Wang, B., Fang, J., Lang, J., Tian, G., Jiang, J., Zhu, T.F., 2014. Inhalable microorganisms in Beijing's $PM_{2.5}$ and PM_{10} pollutants during a severe smog event. Environ Sci Technol. 48, 1499-1507.

Cao, J., Xu, H., Xu, Q., Chen, B., Kan, H., 2012. Fine particulate matter constituents and cardiopulmonary mortality in a heavily polluted Chinese city. Environ Health Persp. 120, 373-378.

Chai, G., He, H., Sha, Y., Zhai, G., Zong, S., 2019. Effect of $PM_{2.5}$ on daily outpatient visits for respiratory diseases in Lanzhou, China. Sci Total Environ. 649, 1563-1572.

Chan, C.K., Yao, X., 2008. Air pollution in megacities in China. Atmos Environ. 42, 1-42.

Chang Graham, A.L., Profeta, L.T.M., Johnson, T.J., Yokelson, R.J., Laskin, A., Laskin, J., 2011. Case study of water soluble metal containing organic constituents of biomass burning aerosol. Environ Sci Technol. 45, 1257-1263.

Chen, H., Yang, S., Li, Y., Yin, Y., Zhang, Z., Yu, X., Kang, N., Yan,Q., Xia, H., 2016. Hygroscopic properties and closure of aerosol chemical composition in Mt. Huang in summer. Environ Sci. 37, 2008-2016. (In Chinese with English abstract)

Chen, J., Zhao, C.S., Ma, N., Liu, P.F., Goebel, T., Hallbauer, E., Deng, Z.Z., Ran, L., Xu, W.Y., Liang, Z., Liu, H.J., Yan, P., Zhou, X.J., Wiedensohler, A., 2012a. A parameterization of low visibilities for hazy days in the North China Plain. Atmos Chem

Phys. 12, 4935-4950.

Chen, L., Peng, C., Gu, W., Fu, H., Jian, X., Zhang, H., Zhang, G., Zhu, J., Wang, X., Tang, M., 2020a. On mineral dust aerosol hygroscopicity. Atmos Chem Phys. 20, 13611-13626.

Chen, R., Kan, H., Chen, B., Huang, W., Bai, Z., Song, G., Pan, G., Grp, C.C., 2012b. Association of particulate air pollution with daily mortality. Am J Epidemiol. 175, 1173-1181.

Chen, S., Xu, L., Zhang, Y., Chen, B., Wang, X., Zhang, X., Zheng, M., Chen, J., Wang, W., Sun, Y., Fu, P., Wang, Z., Li, W., 2017a. Direct observations of organic aerosols in common wintertime hazes in North China: insights into direct emissions from Chinese residential stoves. Atmos Chem Phys. 17, 1258-1270.

Chen, X., Wang, T., Qiu, X., Que, C., Zhang, H., Zhang, L., Zhu, T., 2020b. Susceptibility of individuals with chronic obstructive pulmonary disease to air pollution exposure in Beijing, China: A case-control panel study (COPDB). Sci Total Environ. 717, 137285.

Chen, Y., Wenger, J.C., Yang, F., Cao, J., Huang, R., Shi, G., Zhang, S., Tian, M., Wang, H., 2017b. Source characterization of urban particles from meat smoking activities in Chongqing, China using single particle aerosol mass spectrometry. Environ Pollut. 228, 92-101.

Cheng, X., Pu, Y., Gu, R., 2020. Effect of Shanxi pilot emission trading scheme on industrial soot and dust emissions: A synthetic control method. Energ Environ-UK. 31, 461-478.

Cheung, H.C., Chou, C.C.K., Lee, C.S.L., Kuo, W.-C., Chang, S.-C., 2020. Hygroscopic properties and cloud condensation nuclei activity of atmospheric aerosols under the influences of Asian continental outflow and new particle formation at a coastal site in eastern Asia. Atmos Chem Phys. 20, 5911-5922.

Chi, J., Li, W., Zhang, D., Zhang, J., Lin, Y., Shen, X., Sun, J., Chen, J., Zhang, X., Zhang, Y., Wang, W., 2015. Sea salt aerosols as a reactive surface for inorganic and organic acidic gases in the Arctic troposphere. Atmos Chem Phys. 15, 11341-11353.

China, S., Mazzoleni, C., Gorkowski, K., Aiken, A.C., Dubey, M.K., 2013. Morphology and mixing state of individual freshly emitted wildfire carbonaceous particles. Nat Commun. 4, 2122.

Choi, N.R., Lee, J.Y., Ahn, Y.G., Kim, Y.P., 2020. Determination of atmospheric amines at Seoul, South Korea via gas chromatography/tandem mass spectrometry. Chemosphere. 258, 127367.

Daigle, C.C., Chalupa, D.C., Gibb, F.R., Morrow, P.E., Oberdorster, G., Utell, M.J., Frampton, M.W., 2003. Ultrafine particle deposition in humans during rest and exercise. Inhal Toxicol. 15, 539-552.

De Bock, L.A., Van Malderen, H., Van Grieken, R.E., 1994. Individual aerosol particle composition variations in air masses crossing the north sea. Environ Sci Technol. 28, 1513-1520.

Dehghani, S., Moore, F., Akhbarizadeh, R., 2017. Microplastic pollution in deposited urban dust, Tehran metropolis, Iran. Environ Sci Pollut R. 24, 20360-20371.

Deng, W., Liu, T., Zhang, Y., Situ, S., Hu, Q., He, Q., Zhang, Z., Lü, S., Bi, X., Wang, X., Boreave, A., George, C., Ding, X., and Wang, X., 2017. Secondary organic aerosol formation from photo-oxidation of toluene with NOx and SO_2: Chamber simulation with purified air versus urban ambient air as matrix, Atmos Environ. 150, 67–76.

Ding, X., Wang, X., Zheng, M., 2011. The influence of temperature and aerosol acidity on biogenic secondary organic aerosol tracers: Observations at a rural site in the central Pearl River Delta region, South China. Atmos Environ. 45, 1303-1311.

Dockery, D.W., Pope, C.A., 3rd, 1994. Acute respiratory effects of particulate air pollution. Annu Rev Publ Health. 15, 107-132.

Dockery, D.W., Pope, C.A., 3rd, Xu, X., Spengler, J.D., Ware, J.H., Fay, M.E., Ferris, B.G., Jr., Speizer, F.E., 1993. An association between air pollution and mortality in six U.S. cities. The New England journal of medicine. 329, 1753-1759.

Donahue, N.M., Henry, K.M., Mentel, T.F., Kiendler-Scharr, A., Spindler, C., Bohn, B., Brauers, T., Dorn, H.P., Fuchs, H., Tillmann, R., Wahner, A., Saathoff, H.,

941 Naumann, K.H., Moehler, O., Leisner, T., Mueller, L., Reinnig, M.C., Hoffmann, T.,
942 Salo, K., Hallquist, M., Frosch, M., Bilde, M., Tritscher, T., Barmet, P., Praplan, A.P.,
943 DeCarlo, P.F., Dommen, J., Prevot, A.S.H., Baltensperger, U., 2012. Aging of biogenic
944 secondary organic aerosol via gas-phase OH radical reactions. P Natl Acad Sci USA.
945 109, 13503-13508.
946 Dong, Z., Kang, S., Qin, D., Shao, Y., Ulbrich, S., Qin, X., 2018. Variability in
947 individual particle structure and mixing states between the glacier-snowpack and
948 atmosphere in the northeastern Tibetan Plateau. Cryosphere. 12, 3877-3890.
949 Ebert, M., Weigel, R., Kandler, K., Guenther, G., Molleker, S., Grooss, J.U., Vogel,
950 B., Weinbruch, S., Borrmann, S., 2016. Chemical analysis of refractory stratospheric
951 aerosol particles collected within the arctic vortex and inside polar stratospheric clouds.
952 Atmos Chem Phys. 16, 8405-8421.
953 Fan, J., Shao, L., Hu, Y., Wang, J., Wang, J., Ma, J., 2016a. Classification and
954 chemical compositions of individual particles at an eastern marginal site of Tibetan
955 Plateau. Atmos Pollut Res. 7, 833-842.
956 Fan, J., Wang, Y., Rosenfeld, D., Liu, X., 2016b. Review of Aerosol Cloud
957 interactions: mechanisms, significance, and challenges. J Atmos Sci. 73, 4221-4252.
958 Frank, E.R., Lodge, J.P., 1967. Morphological identification of air borne particles
959 with electron miscroscope. J Microsc-Oxford. 6, 449-456.
960 Fraund, M., Park, T., Yao, L., Bonanno, D., Pham, D.Q., Moffet, R.C., 2019.
961 Quantitative capabilities of STXM to measure spatially resolved organic volume
962 fractions of mixed organic/inorganic particles. Atmos Meas Tech. 12, 1619-1633.
963 Freney, E.J., Adachi, K., Buseck, P.R., 2010. Internally mixed atmospheric aerosol
964 particles: Hygroscopic growth and light scattering. J Geophys Res-Atmos. 115, D19210.
965 Frey, M.M., Norris, S.J., Brooks, I.M., Anderson, P.S., Nishimura, K., Yang, X.,
966 Jones, A.E., Mastromonaco, M.G.N., Jones, D.H., Wolff, E.W., 2020. First direct
967 observation of sea salt aerosol production from blowing snow above sea ice. Atmos
968 Chem Phys. 20, 2549-2578.
969 Fuzzi, S., Andreae, M.O., Huebert, B.J., Kulmala, M., Bond, T.C., Boy, M.,

970 Doherty, S.J., Guenther, A., Kanakidou, M., Kawamura, K., Kerminen, V.M., Lohmann,
971 U., Russell, L.M., Poeschl, U., 2006. Critical assessment of the current state of scientific
972 knowledge, terminology, and research needs concerning the role of organic aerosols in
973 the atmosphere, climate, and global change. Atmos Chem Phys. 6, 2017-2038.
974 Garcia Hernandez, C., Ferrero, A., Estarlich, M., Ballester, F., 2019. Exposure to
975 ultrafine particles in children until 18 years of age: A systematic review. Indoor Air. 30,
976 7-23.
977 Gard, E., Mayer, J.E., Morrical, B.D., 1997. Real-time analysis of individual
978 atmospheric aerosol particles: design and performance of a portable ATOFMS. Anal
979 Chem. 69, 4083-4091.
980 Gasparini, R., Li, R.J., Collins, D.R., 2004. Integration of size distributions and
981 size-resolved hygroscopicity measured during the Houston Supersite for compositional
982 categorization of the aerosol. Atmos Environ. 38, 3285-3303.
983 Georgakakou, S., Gourgoulianis, K., Daniil, Z., Bontozoglou, V., 2016. Prediction
984 of particle deposition in the lungs based on simple modeling of alveolar mixing. Resp
985 Physiol Neurobi. 225, 8-18.
986 Ghosal, S., Weber, P.K., Laskin, A., 2014. Spatially resolved chemical imaging of
987 individual atmospheric particles using nanoscale imaging mass spectrometry: insight
988 into particle origin and chemistry. Anal Methods-UK. 6, 2444-2451.
989 Giordano, M., Espinoza, C., Asa-Awuku, A., 2015. Experimentally measured
990 morphology of biomass burning aerosol and its impacts on CCN ability. Atmos Chem
991 Phys. 15, 1807-1821.
992 Han, L., Sun, Z., He, J., Hao, Y., Tang, Q., Zhang, X., Zheng, C., Miao, S., 2020.
993 Seasonal variation in health impacts associated with visibility in Beijing, China. Sci
994 Total Environ. 730, 139149.
995 He, J., Hu, Q., Jiang, M., Huang, Q., 2021. Nanostructure and reactivity of soot
996 particles from open burning of household solid waste, Chemosphere. 269, 129395.
997 Hennigan, C.J., Miracolo, M.A., Engelhart, G.J., May, A.A., Presto, A.A., Lee, T.,
998 Sullivan, A.P., McMeeking, G.R., Coe, H., Wold, C.E., Hao, W.M., Gilman, J.B., Kuster,

W.C., de Gouw, J., Schichtel, B.A., Collett, J.L., Jr., Kreidenweis, S.M., Robinson, A.L., 2011. Chemical and physical transformations of organic aerosol from the photo-oxidation of open biomass burning emissions in an environmental chamber. Atmos Chem Phys. 11, 7669-7686.

Heringa, M.F., DeCarlo, P.F., Chirico, R., Tritscher, T., Dommen, J., Weingartner, E., Richter, R., Wehrle, G., Prevot, A.S.H., Baltensperger, U., 2011. Investigations of primary and secondary particulate matter of different wood combustion appliances with a high-resolution time-of-flight aerosol mass spectrometer. Atmos Chem Phys. 11, 5945-5957.

Hou, C., 2017. Study on individual and aging process of individual particle in $PM_{2.5}$ in highway tunnel and urban Road. Ph D thesis of China University of Mining & Technology, Beijing. (In Chinese with English abstract)

Hou, C., Shao, L., Hu, W., Zhang, D., Zhao, C., Xing, J., Huang, X., Hu, M., 2018. Characteristics and aging of traffic-derived particles in a highway tunnel at a coastal city in southern China. Sci Total Environ. 619, 1385-1393.

Hou, C., Shao, L., Hu, W., Zhang, D., Zhao, C., Xing, J., Huang, X., Hu, M., 2018a. Characteristics and aging of traffic-derived particles in a highway tunnel at a coastal city in southern China. Sci Total Environ. 619, 1385-1393.

Hou, C., Shao, L., Zhao, C., Wang, J., Liu, J., Geng, C., 2018b. Characterization of coal burning derived individual particles emitted from an experimental domestic stove. J Environ Sci. 71, 45-55.

Hu, T., Cao, J., Zhu, C., Zhao, Z., Liu, S., Zhang, D., 2018. Morphologies and elemental compositions of local biomass burning particles at urban and glacier sites in Southeastern Tibetan Plateau: Results from an expedition in 2010. Sci Total Environ. 628, 772-781.

Huang, R.J., Zhang, Y., Bozzetti, C., Ho, K.-F., Cao, J.J., Han, Y., Daellenbach, K.R., Slowik, J.G., Platt, S.M., Canonaco, F., Zotter, P., Wolf, R., Pieber, S.M., Bruns, E.A., Crippa, M., Ciarelli, G., Piazzalunga, A., Schwikowski, M., Abbaszade, G., Schnelle-Kreis, J., Zimmermann, R., An, Z., Szidat, S., Baltensperger, U., El Haddad,

I., Prevot, A.S.H., 2014. High secondary aerosol contribution to particulate pollution during haze events in China. Nature. 514, 218-222.

Hwa, M.Y., Yu, T.Y., 2014. Development of real-world driving cycles and estimation of emission factors for in use light duty gasoline vehicles in urban areas. Environ Monit Assess. 186, 3985-3994.

Iwasaka, Y., Yamato, M., Imasu, R., Ono, A., 1988. Transport of Asian dust (KOSA) particles; Importance of weak KOSA enevts on the geochemical cycle of soil particles, Tellus. 40B, 494-503.

Jones, E.R., Laurent, J.G.C., Young, A.S., MacNaughton, P., Coull, B.A., Spengler, J.D., Allen, J.G., 2021. The effects of ventilation and filtration on indoor PM2.5 in office buildings in four countries. Build Environ. 200, 107975.

Jane, K., Amber, G., 2015. Tracking long range atmospheric transport of contaminants in Arctic regions using lake sediments. Environmental Contaminants. 8, 223-262.

Jaoui, M., Kleindienst, T.E., Offenberg, J.H., Lewandowski, M., Lonneman, W.A., 2012. SOA formation from the atmospheric oxidation of 2-methyl-3-buten-2-ol and its implications for $PM_{2.5}$. Atmos Chem Phys. 12, 2173-2188.

Jones, T., Wlodarczyk, A., Koshy, L., Brown, P., Longyi, S., BeruBe, K., 2009. The geochemistry and bioreactivity of fly-ash from coal burning power stations. Biomarkers. 14, 45-48.

Jones, T.P., Williamson, B.J., BeruBe, K.A., Richards, R.J., 2001. Microscopy and chemistry of particles collected on TEOM filters: Swansea, south Wales, 1998-1999. Atmos Environ. 35, 3573-3583.

Karydis, V.A., Tsimpidi, A.P., Bacer, S., Pozzer, A., Nenes, A., Lelieveld, J., 2017. Global impact of mineral dust on cloud droplet number concentration. Atmos Chem Phys. 17, 5601-5621.

Kashiwakura, S., Ohno, H., Matsubae-Yokoyarna, K., Kumagai, Y., Kubo, H., Nagasaka, T., 2010. Removal of arsenic in coal fly ash by acid washing process using dilute H_2SO_4 solvent. J Hazard Mater. 181, 419-425.

Katrinak, K.A., Anderson, J.R., Buseck, P.R., 1995. Individual particle types in the aerosol of phoenix, Arizona. Environ Sci Technol. 29, 321-329.

Krishnamohan, K.S., Bala, G., Cao, L., Duan, L., Caldeira, K., 2020. The climatic effects of hygroscopic growth of sulfate aerosols in the Stratosphere. Earths Future. 8, UNSP e2019EF001326.

Kuwata, M., Martin, S.T., 2012. Phase of atmospheric secondary organic material affects its reactivity. P Natl Acad Sci USA. 109, 17354-17359.

Lambert, F., Delmonte, B., Petit, J.R., Bigler, M., Kaufmann, P.R., Hutterli, M.A., Stocker, T.F., Ruth, U., Steffensen, J.P., Maggi, V., 2008. Dust-climate couplings over the past 800,000 years from the EPICA Dome C ice core. Nature. 452, 616-619.

Laskin, A., Laskin, J., Nizkorodov, S.A., 2015. chemistry of atmospheric brown carbon. Chem Rev. 115, 4335-4382.

Lawson, M.J., Prytherch, Z.C., Jones, T.P., Adams, R.A., BeruBe, K.A., 2020. Iron-rich magnetic coal fly ash particles induce apoptosis in human bronchial cells. Appl Sci-Basel. 10, 8363.

Lazzeri, R., Clauser, G., Iacob, E., Lui, A., Tonidandel, G., Anderle, M., 2003. ToF-SIMS and XPS characterisation of urban aerosols for pollution studies. Appl Surf Sci. 203, 767-771.

Le Roux, G., Fagel, N., De Vleeschouwer, F., Krachler, M., Debaille, V., Stille, P., Mattielli, N., van der Knaap, W.O., van Leeuwen, J.F.N., Shotyk, W., 2012. Volcano and climate driven changes in atmospheric dust sources and fluxes since the Late Glacial in Central Europe. Geology. 40, 335-338.

Lei, T., Zuend, A., Wang, W.G., Zhang, Y.H., Ge, M.F., 2014. Hygroscopicity of organic compounds from biomass burning and their influence on the water uptake of mixed organic ammonium sulfate aerosols. Atmos Chem Phys. 14, 11165-11183.

Lelieveld, J., Pozzer, A., Poeschl, U., Fnais, M., Haines, A., Muenzel, T., 2020. Loss of life expectancy from air pollution compared to other risk factors: a worldwide perspective. Cardiovasc Res. 116, 1910-1917.

Li, J., Posfai, M., Hobbs, P.V., Buseck, P.R., 2003. Individual aerosol particles

from biomass burning in southern Africa: 2, Compositions and aging of inorganic particles. J Geophys Res-Atmos. 108, 8484.

Li, K., Sinha, B., Hoppe, P., 2016a. Speciation of nitrogen-bearing species using negative and positive secondary ion spectra with nano secondary ion mass spectrometry. Anal Chem. 88, 3281-3288.

Li, S., Ma.Yan, Zheng, J., Yao, L., Zhou, Y., Wang, Z., 2015. Physicochemical properties of secondary organic aerosols and cloud condensation activity in ozone oxidation of α-pinene. Environ Chem. 34, 1633-1641. (In Chinese with English abstract)

Li, W., Liu, L., Xu, L., Zhang, J., Yuan, Q., Ding, X., Hu, W., Fu, P., Zhang, D., 2020a. Overview of primary biological aerosol particles from a Chinese boreal forest: Insight into morphology, size, and mixing state at microscopic scale. Sci Total Environ. 719, 137520.

Li, W., Liu, L., Zhang, J., Xu, L., Wang, Y., Sun, Y. and Shi, Z., 2021. Microscopic evidence for phase separation of organic species and inorganic salts in fine ambient aerosol particles. Environ Sci Techn. 55, 2234-2242.

Li, W., Shao, L., 2009a. Transmission electron microscopy study of aerosol particles from the brown hazes in northern China. J Geophys Res-Atmos. 114, D09302.

Li, W., Shao, L., 2009b. Observation of nitrate coatings on atmospheric mineral dust particles. Atmos Chem Phys. 9, 1863-1871.

Li, W., Shao, L., 2010. Characterization of mineral particles in winter fog of Beijing analyzed by TEM and SEM. Environ Monit Assess. 161, 565-573.

Li, W., Shao, L., Shen, R., Yang, S., Wang, Z., Tang, U., 2011. Internally mixed sea salt, soot, and sulfates at macao, a coastal city in South China. J Air Waste Manage. 61, 1166-1173.

Li, W., Shao, L., 2013. Study on Individual Aerosol Particles in Fog, Brown Haze, and Dust Storm Episodes. Science Press. Beijing. 146pp.

Li, W., Shao, L., Shi, Z., Chen, J., Yang, L., Yuan, Q., Yan, C., Zhang, X., Wang, Y., Sun, J., Zhang, Y., Shen, X., Wang, Z., Wang, W., 2014. Mixing state and hygroscopicity of dust and haze particles before leaving Asian continent. J Geophys

Res-Atmos. 119, 1044-1059.

Li, W., Shao, L., Wang, W., Li, H., Wang, X., Li, Y., Li, W., Jones, T., Zhang, D., 2020b. Air quality improvement in response to intensified control strategies in Beijing during 2013-2019. Sci Total Environ. 744, 140776.

Li, W., Shao, L., Wang, Z., Shen, R., Yang, S., Tang, U., 2010a. Size, composition, and mixing state of individual aerosol particles in a South China coastal city. J Environ Sci. 22, 561-569.

Li, W., Shao, L., Zhang, D., Ro, C.U., Hu, M., Bi, X., Geng, H., Matsuki, A., Niu, H., Chen, J., 2016b. A review of single aerosol particle studies in the atmosphere of East Asia: morphology, mixing state, source, and heterogeneous reactions. J Clean Prod. 112, 1330-1349.

Li, W., Sun, J., Xu, L., Shi, Z., Riemer, N., Sun, Y., Fu, P., Zhang, J., Lin, Y., Wang, X., Shao, L., Chen, J., Zhang, X., Wang, Z., Wang, W., 2016c. A conceptual framework for mixing structures in individual aerosol particles. J Geophys Res-Atmos. 121, 13784-13798.

Li, W., Wang, T., Zhou, S., Lee, S., Huang, Y., Gao, Y., Wang, W., 2013a. Microscopic observation of metal-containing particles from Chinese continental outflow observed from a non-industrial site. Environ Sci Technol. 47, 9124-9131.

Li, W., Xu, L., Liu, X., Zhang, J., Lin, Y., Yao, X., Gao, H., Zhang, D., Chen, J., Wang, W., Harrison, R.M., Zhang, X., Shao, L., Fu, P., Nenes, A., Shi, Z., 2017. Air pollution-aerosol interactions produce more bioavailable iron for ocean ecosystems. Sci Adv. 3, e1601749.

Li, W., Shao, L., Buseck, P.R., 2010b. Haze types in Beijing and the influence of agricultural biomass burning. Atmos Chem Phys. 10, 8119-8130.

Li, X., Wang, S., Duan, L., Hao, J., Li, C., Chen, Y., Yang, L., 2007. Particulate and trace gas emissions from open burning of wheat straw and corn stover in China. Environ Sci Technol. 41, 6052-6058.

Li, Y., 2021. Characteristics and aging process of individual aerosol particles emitted from biomass and residential coal combustion. Ph D thesis of China University

of Mining & Technology, Beijing. (In Chinese with English abstract)

Li, Z., Shao, L., Fan, J., Hu, Y., Hou, C., 2013b. Morphology and elemental composition of individual particles under different weather conditions in Beijing. China Environ Sci. 33, 1546-1552. (In Chinese with English abstract)

Liati, A., Schreiber, D., Eggenschwiler, P.D., Dasilva, Y.A.R., 2013. Metal particle emissions in the exhaust stream of diesel engines: an electron microscope study. Environ Sci Technol. 47, 14495-14501.

Liu, T., Wang, X., Deng, W., Hu, Q., Ding, X., Zhang, Y., He, Q., Zhang, Z., Lü, S., Bi, X., Chen, J., and Yu, J., 2015. Secondary organic aerosol formation from photochemical aging of light-duty gasoline vehicle exhausts in a smog chamber. Atmos Chem Phys. 15, 9049–9062.

Liu, X., Jia, H., Qi, J., Zhang, J., Ma, Q., 1994. Scanning electron microscope study and pollution source identification of atmospheric particulate matter in Qingdao. Res Environ Sci. 7, 10-17. (In Chinese with English abstract)

Liu, L., Kong, S., Zhang, Y., Wang, Y., Xu, L., Yan, Q., Lingaswamy, A.P., Shi, Z., Lv, S., Niu, H., Shao, L., Hu, M., Zhang, D., Chen, J., Zhang, X., Li, W., 2017. Morphology, composition, and mixing state of primary particles from combustion sources - crop residue, wood, and solid waste. Sci Rep-UK. 7, 5047.

Liu, L., Zhang, J., Xu, L., Yuan, Q., Huang, D., Chen, J., Shi, Z., Sun, Y., Fu, P., Wang, Z., Zhang, D., Li, W., 2018. Cloud scavenging of anthropogenic refractory particles at a mountain site in North China. Atmos Chem Phys. 18, 14681-14693.

Liu, X., Zhang, Y., 2010. Advances in research on aerosol hygroscopic properties at home and abroad. Climatic Environ Res. 6, 806-816. (In Chinese with English abstract)

Liu, Y., Sun, J., Yang, B., 2009. The effects of black carbon and sulphate aerosols in China regions on East Asia monsoons. Tellus B. 61, 642-656.

Liu, Y., Wu, Z., Huang, X., Shen, H., Bai, Y., Qiao, K., Meng, X., Hu, W., Tang, M., He, L., 2019. Aerosol phase state and its link to chemical composition and liquid water content in a subtropical coastal megacity. Environ Sci Technol. 53, 5027-5033.

Lu, S., Tan, Z., Liu, P., Zhao, H., Liu, D., Yu, S., Cheng, P., Win, M.S., Hu, J., Tian, L., Wu, M., Yonemochi, S., Wang, Q., 2017. Single particle aerosol mass spectrometry of coal combustion particles associated with high lung cancer rates in Xuanwei and Fuyuan, China. Chemosphere. 186, 278-286.

Luo, X., Bing, H., Luo, Z., Wang, Y., Jin, L., 2019. Impacts of atmospheric particulate matter pollution on environmental biogeochemistry of trace metals in soil-plant system: A review. Environ Pollut. 255, 113138.

Mahowald, N.M., Hamilton, D.S., Mackey, K.R.M., Moore, J.K., Baker, A.R., Scanza, R.A., Zhang, Y., 2018. Aerosol trace metal leaching and impacts on marine microorganisms. Nat Commun. 9, 2614.

Maji, S., Beig, G., Yadav, R., 2020. Winter VOCs and OVOCs measured with PTR-MS at an urban site of India: Role of emissions, meteorology and photochemical sources. Environ Pollut. 258, 113651.

Mamane, Y., Noll, K.E.J.A.E., 1985. Characterization of large particles at a rural site in the eastern United States: Mass distribution and individual particle analysis. Atmos Environ. 19, 611-622.

Manigrasso, M., Capannesi, G., Rosada, A., Lammardo, M., Ceci, P., Petrucci, A., Avino, P., 2020. Deep inorganic fraction characterization of PM_{10}, $PM_{2.5}$, and PM_1 in an industrial area located in central Italy by means of instrumental neutron activation analysis. Appl Sci-Basel. 10, 2532.

Manigrasso, M., Protano, C., Astolfi, M.L., Massimi, L., Avinod, P., Vitali, M., Canepari, S., 2019. Evidences of copper nanoparticle exposure in indoor environments: Long term assessment, high resolution field emission scanning electron microscopy evaluation, in silico respiratory dosimetry study and possible health implications. Sci Total Environ. 653, 1192-1203.

McInnes, L.M., Covert, D.S., Quinn, P.K., Germani, M.S., 1994. Measurements of chloride depletion and sulfur enrichment in individual sea salt particles collected from the remote marine boundary layer. J Geophys Res. 99, 8257-8268.

McMeeking, G.R., Morgan, W.T., Flynn, M., Highwood, E.J., Turnbull, K.,

Haywood, J., Coe, H., 2011. Black carbon aerosol mixing state, organic aerosols and aerosol optical properties over the United Kingdom. Atmos Chem Phys. 11, 9037-9052.

McNeill, V.F., 2017. Atmospheric aerosols: clouds, chemistry, and climate, in: Prausnitz, J.M. (Ed.). Annu Rev Chem Biomol. 8, 427-444.

Meesang, W., Bualert, S., Wonglakorn, P., 2013. Sea salt aerosols: Shortwave radiative forcing. Int J Environ Sci Dev. 4, 104-106.

Menzel, N., Schramel, P., Wittmaack, K., 2002. Elemental composition of aerosol particulate matter collected on membrane filters: A comparison of results by PIXE and ICP-AES. Nucl Instrum Meth B. 189, 94-99.

Middlebrook, A.M., Murphy, D.M., Lee, S.H., Thomson, D.S., Prather, K.A., Wenzel, R.J., Liu, D.Y., Phares, D.J., Rhoads, K.P., Wexler, A.S., Johnston, M.V., Jimenez, J.L., Jayne, J.T., Worsnop, D.R., Yourshaw, I., Seinfeld, J.H., Flagan, R.C., 2003. A comparison of particle mass spectrometers during the 1999 Atlanta Supersite Project. J Geophys Res-Atmos. 108, 8424.

Miracolo, M.A., Hennigan, C.J., Ranjan, M., Nguyen, N.T., Gordon, T.D., Lipsky, E.M., Presto, A.A., Donahue, N.M., Robinson, A.L., 2011. Secondary aerosol formation from photochemical aging of aircraft exhaust in a smog chamber. Atmos Chem Phys. 11, 4135-4147.

Moreno, T., Martins, V., Querol, X., Jones, T., BeruBe, K., Cruz Minguillon, M., Amato, F., Capdevila, M., de Miguel, E., Centelles, S., Gibbons, W., 2015. A new look at inhalable metalliferous airborne particles on rail subway platforms. Sci Total Environ. 505, 367-375.

Mu, Z., Chen, Q., Zhang, L., Guan, D., Li, H., 2021. Photodegradation of atmospheric chromophores: changes in oxidation state and photochemical reactivity. Atmos Chem Phys. 21, 11581-11591.

Naing, N.N., Lee, H.K., 2020. Microextraction and analysis of contaminants adsorbed on atmospheric fine particulate matter: A review. J Chromatogr A. 1627, 461433.

Niu, H., Shao, L., Zhang, D., 2011. Aged status of soot particles during the passage

of a weak cyclone in Beijing. Atmos Environ. 45, 2699-2703.

Niu, H., Shao, L., Zhang, D., 2012. Soot particles at an elevated site in eastern China during the passage of a strong cyclone. Sci Total Environ. 430, 217-222.

Oberdorster, G., Gelein, R.M., Ferin, J., Weiss, B., 1995. Association of particulate air pollution and acute mortality: involvement of ultrafine particles? Inhal Toxicol. 7, 111-124.

Oberdorster, G., Sharp, Z., Atudorei, V., Elder, A., Gelein, R., Kreyling, W., Cox, C., 2004. Translocation of inhaled ultrafine particles to the brain. Inhal Toxicol. 16, 437-445.

Okada, K., Qin, Y., Kai, K., 2005. Elemental composition and mixing properties of atmospheric mineral particles collected in Hohhot, China. Atmos Res. 73, 45-67.

Oliveira, M.L.S., Flores, E.M.M., Dotto, G. L., Neckel, A., Silva, L.F.O., 2021. Nanomineralogy of mortars and ceramics from the Forum of Caesar and Nerva (Rome, Italy): The protagonist of black crusts produced on historic buildings. J Clean Prod. 278, 123982.

Ono, K., Mizushima, Y., Furuya, M., Kunihisa, R., Tsuchiya, N., Fukuma, T., Iwata, A., Matsuki, A., 2020. Direct measurement of adhesion force of individual aerosol particles by atomic force microscopy. Atmosphere. 11, 489.

Peng, L., Li, L., Lin, Q., Li, M., Zhang, G., Bi, X., Wang, X., Sheng, G., 2020. Does atmospheric processing produce toxic Pb-containing compounds? A case study in suburban Beijing by single particle mass spectrometry. J Hazard Mater. 382, 121014.

Penner, J.E., Dickinson, R.E., O'Neill, C.A., 1992. Effects of aerosol from biomass burning on the global radiation budget. Science (New York, N.Y.). 256, 1432-1434.

Petters, M.D., Kreidenweis, S.M., 2007. A single parameter representation of hygroscopic growth and cloud condensation nucleus activity. Atmos Chem Phys. 7, 1961-1971.

Pinedo Gonzalez, P., Hawco, N.J., Bundy, R.M., Armbrust, E.V., Follows, M.J., Cael, B.B., White, A.E., Ferron, S., Karl, D.M., John, S.G., 2020. Anthropogenic Asian aerosols provide Fe to the North Pacific Ocean. P Natl Acad Sci USA. 117, 27862-

27868.

Pope, C.A., 3rd, Thun, M.J., Namboodiri, M.M., Dockery, D.W., Evans, J.S., Speizer, F.E., Heath, C.W., Jr., 1995. Particulate air pollution as a predictor of mortality in a prospective study of U.S. adults. Am J Resp Crit Care. 151, 669-674.

Pope, C.A., III, Dockery, D.W., 2006. Health effects of fine particulate air pollution: Lines that connect. J Air Waste Manage. 56, 709-742.

Poschl, U., 2005. Atmospheric aerosols: Composition, transformation, climate and health effects. Angew Chem Int Edit. 44, 7520-7540.

Posfai, M., Axisa, D., Tompa, E., Freney, E., Bruintjes, R., Buseck, P.R., 2013a. Interactions of mineral dust with pollution and clouds: An individual particle TEM study of atmospheric aerosol from Saudi Arabia. Atmos Res. 122, 347-361.

Posfai, M., Buseck, P.R., 2010. Nature and climate effects of individual tropospheric aerosol particles, in: Jeanloz, R., Freeman, K.H. (Eds.). Annu Rev Earth Pl Sc.38, 17-43.

Posfai, M., Gelencser, A., Simonics, R., Arato, K., Li, J., Hobbs, P.V., Buseck, P.R., 2004. Atmospheric tar balls: Particles from biomass and biofuel burning. J Geophys Res-Atmos. 109, D06213.

Posfai, M., Kasama, T., Dunin Borkowski, R.E., 2013b. Biominerals at the nanoscale: transmission electron microscopy methods for studying the special properties of biominerals, 13th EMU School, Univ Granada, Granada, Spain, 14, 377-435.

Prospero, J.M., 1999. Long-range transport of mineral dust in the global atmosphere: impact of African dust on the environment of the southeastern United States. P Natl Acad Sci USA. 96, 3396-3403.

Pui, D.Y.H., Chen, S. C., Zuo, Z., 2014. $PM_{2.5}$ in China: Measurements, sources, visibility and health effects, and mitigation. Particuology. 13, 1-26.

Ramírez, O., da Boit, K., Blanco, E., Silva, L.F.O., 2020. Hazardous thoracic and ultrafine particles from road dust in a Caribbean industrial city. Urban Clim. 33, 100655.

Ramsden, A.R., Shibaoka, M.J.A.E., 1982. Characterization and analysis of

1289 individual fly ash particles from coal-fired power stations by a combination of optical
1290 microscopy, electron microscopy and quantitative electron microprobe analysis. Atmos
1291 Environ. 16, 2191-2195.
1292 Reyes Villegas, E., Bannan, T., Le Breton, M., Mehra, A., Priestley, M., Percival,
1293 C., Coe, H., Allan, J.D., 2018. Online chemical characterization of food cooking
1294 organic aerosols: Implications for source apportionment. Environ Sci Technol. 52,
1295 5308-5318.
1296 Richards, R., 2003. What effects do mineral particles have in the lung? Mineral
1297 Mag. 67, 129-139.
1298 Richards, R.J., Atkins, J., Marrs, T.C., Brown, R., Masek, L.J.T., 1989. The
1299 biochemical and pathological changes produced by the intratracheal instillation of
1300 certain components of zinc-hexachloroethane smoke. Toxicol Lett. 54, 79-88.
1301 Rodriguez, E.S., Perron, M.M.G., Strzelec, M., Proemse, B.C., Bowie, A.R., Paull,
1302 B., 2020. Analysis of levoglucosan and its isomers in atmospheric samples by ion
1303 chromatography with electrospray lithium cationisation-triple quadrupole tandem mass
1304 spectrometry. J Chromatogr A. 1610, 460557.
1305 Saikia, B.K., Saikia, J., Rabha, S., Silva, L.F., Finkelman, R., 2018. Ambient
1306 nanoparticles/nanominerals and hazardous elements from coal combustion activity:
1307 Implications on energy challenges and health hazards. Geosci Front. 9, 863-875.
1308 Shao, L., Hu, Y., Fan, J., Wang, J., Wang, J., Ma, J., 2017. Physicochemical
1309 characteristics of aerosol particles in the Tibetan Plateau: Insights from TEM-EDX
1310 analysis. J Nanosci Nanotechno. 17, 6899-6908.
1311 Shao, L., Li, J., Zhao, H., Yang, S., Li, H., Li, W., Jones, T., Sexton, K.,
1312 Environment, K.B.J.A., 2007. Associations between particle physicochemical
1313 characteristics and oxidative capacity: An indoor PM_{10} study in Beijing, China. Atmos
1314 Environ. 41, 5316-5326.
1315 Shao, L., Shi, Z., 2000. Study on inhalable particulate matter in urban atmosphere.
1316 Environ Prot. 1, 24-29. (In Chinese with English abstract)
1317 Shao, L., Shi, Z., Jones, T.P., Li, J., Whittaker, A.G., Berube, K.A., 2006a.

Bioreactivity of particulate matter in Beijing air: Results from plasmid DNA assay. Sci Total Environ. 367, 261-272.

Shao, L., Yang, S., Shi, Z., Lv, S. 2006b. A Study on Physico-Chemistry and Bioreactivity of Inhalable Particulates in Urban Air. China Meteorol Press. 209.

Shen, L., Wang, H., Cheng, M., Ji, D., Liu, Z., Wang, L., Gao, W., Yang, Y., Huang, W., Zhang, R., Zou, J., Wang, Y., 2021. Chemical composition, water content and size distribution of aerosols during different development stages of regional haze episodes over the North China Plain. Atmos Environ. 245, 118020.

Shen, L., Wang, H., Gao, W., Yang, Y., Huang, W., Wang, L., Zhang, R., Zou, J., Ji, D., Wang, Y., 2020. Real-time physiochemistry of urban aerosols during a regional haze episode by a single particle aerosol mass spectrometer: Mixing state, size distribution and source apportionment. Atmos Pollut Res. 11, 1329-1338.

Shi, Y., Ji, Y., Sun, H., Hui, F., Hu, J., Wu, Y., Fang, J., Lin, H., Wang, J., Duan, H., Lanza, M., 2015. Nanoscale characterization of $PM_{2.5}$ airborne pollutants reveals high adhesiveness and aggregation capability of soot particles. Sci Rep-UK. 5, 11232.

Shi, Z.B., Shao, L.Y., Jones, T.P., Whittaker, A.G., Lu, S.L., Berube, K.A., He, T., Richards, R.J., 2003. Characterization of airborne individual particles collected in an urban area, a satellite city and a clean air area in Beijing, 2001. Atmos Environ. 37, 4097-4108.

Silva, L.F.O., Santosh, M., Schindler, M., Gasparotto, J., Dotto, G.L., Oliveira, M.L.S., Hochella, M.F., 2021. Nanoparticles in fossil and mineral fuel sectors and their impact on environment and human health: A review and perspective. Gondwana Res. 92, 184-201.

Singh, N., Banerjee, T., Raju, M.P., Deboudt, K., Sorek-Hamer, M., Singh, R.S., Mall, R.K., 2018. Aerosol chemistry, transport, and climatic implications during extreme biomass burning emissions over the Indo-Gangetic Plain. Atmos Chem Phys. 18, 14197-14215.

Slade, J.H., Shiraiwa, M., Arangio, A., Su, H., Poeschl, U., Wang, J., Knopf, D.A., 2017. Cloud droplet activation through oxidation of organic aerosol influenced by

temperature and particle phase state. Geophys Res Lett. 44, 1583-1591.

Stockwell, C.E., Yokelson, R.J., Kreidenweis, S.M., Robinson, A.L., Demott, P.J., Sullivan, R.C., Reardon, J., Ryan, K.C., Griffith, D.W.T., Stevens, L., 2014. Trace gas emissions from combustion of peat, crop residue, domestic biofuels, grasses, and other fuels: configuration and Fourier transform infrared (FTIR) component of the fourth Fire Lab at Missoula Experiment (FLAME-4). Atmos Chem Phys. 14, 9727-9754.

Sun, X., Zhao, T., Liu, D., Gong, S., Xu, J., Ma, X., 2020. Quantifying the influences of $PM_{2.5}$ and relative humidity on change of atmospheric visibility over recent winters in an urban area of east China. Atmosphere. 11, 461.

Sun, Z., Duan, F., He, K., Du, J., Zhu, L., 2019. Sulfate-nitrate-ammonium as double salts in $PM_{2.5}$: Direct observations and implications for haze events. Sci Total Environ. 647, 204-209.

Tang, X., Zhang, Y., Shao, M., 2006. Atmospheric environmental chemistry (2nd Edition). Higher education press. 4, 739.

Tang, M.J., Whitehead, J., Davidson, N.M., Pope, F.D., Alfarra, M.R., McFiggans, G., Kalberer, M., 2015. Cloud condensation nucleation activities of calcium carbonate and its atmospheric ageing products. Phys Chem Chem Phys. 17, 32194-32203.

Tariq, S., Ul Haq, Z., Ali, M., 2016. Satellite and ground-based remote sensing of aerosols during intense haze event of October 2013 over Lahore, Pakistan. Asia-Pac J Atmos Sci. 52, 25-33.

Tervahattu, H., Juhanoja, J., Kupiainen, K., 2002. Identification of an organic coating on marine aerosol particles by TOF-SIMS. J Geophys Res-Atmos. 107, 4319.

The State Council of China, 2013. Air pollution prevention and control action plan. (Accessed 12 September 2013) (In Chinese).

Toner, S.M., Sodeman, D.A., Prather, K.A., 2006. Single particle characterization of ultrafine and accumulation mode particles from heavy duty diesel vehicles using aerosol time-of-flight mass spectrometry. Environ Sci Technol. 40, 3912-3921.

Toner, S.M., Shields, L.G., Sodeman, D.A., Prather, K.A., 2008. Using mass spectral source signatures to apportion exhaust particles from gasoline and diesel

1376 powered vehicles in a freeway study using UF-ATOFMS. Atmos Environ. 42, 568-581.
1377 Trejos, E.M., Silva, L.F.O., Hower, J.C., Flores, E.M., Gonzalez, C.M., Pachon,
1378 J.E., Aristizabal, B.H., 2021. Volcanic emissions and atmospheric pollution: A study of
1379 nanoparticles. Geosci Front. 12, 746-755.
1380 Tsai, Y.I., 2005. Atmospheric visibility trends in an urban area in Taiwan 1961-
1381 2003. Atmos Environ. 39, 5555-5567.
1382 Wang, M.J., Zheng, N., Zhao, D.F., Shang, J., Zhu, T., 2021b. Using micro-raman
1383 spectroscopy to investigate chemical composition, mixing states, and heterogeneous
1384 reactions of individual atmospheric particles. Environ Sci Technol. 55, 10243-10254
1385 Wang, J., Zhang, Q., Chen, M., Collier, S., Zhou, S., Ge, X., Xu, J., Shi, J., Xie,
1386 C., Hu, J., Ge, S., Sun, Y., Coe, H., 2017. First chemical characterization of refractory
1387 black carbon aerosols and associated coatings over the Tibetan Plateau (4730 m a.s.l).
1388 Environ Sci Technol. 51, 14072-14082.
1389 Wang, Q., Cao, J., Han, Y., Tian, J., Zhang, Y., Pongpiachan, S., Zhang, Y., Li, L.,
1390 Niu, X., Shen, Z., Zhao, Z., Tipmanee, D., Bunsomboonsakul, S., Chen, Y., Sun, J.,
1391 2018. Enhanced light absorption due to the mixing state of black carbon in fresh
1392 biomass burning emissions. Atmos Environ. 180, 184-191.
1393 Wang, W., 2020. Individual particle types and aging characteristics of $PM_{2.5}$ under
1394 different pollution weather in Beijing. Ph D thesis of China University of Mining &
1395 Technology, Beijing. (In Chinese with English abstract)
1396 Wang, W., Shao, L., Li, J., Chang, L., Zhang, D., Zhang, C., Jiang, J., 2019a.
1397 Characteristics of individual particles emitted from an experimental burning chamber
1398 with coal from the lung cancer area of Xuanwei, China. Aerosol Air Qual Res. 19, 355-
1399 363.
1400 Wang, W., Shao, L., Zhang, D., Li, Y., Li, W., Liu, P., Xing, J., 2021a.
1401 Mineralogical similarities and differences of dust storm particles at Beijing from deserts
1402 in the north and northwest. Sci Total Environ. 803, 149980.
1403 Wang, Y., Niu, S., Lv, J., Lu, C., Xu, X., Wang, Y., Ding, J., Zhang, H., Wang, T.,
1404 Kang, B., 2019b. A new method for distinguishing unactivated particles in cloud

condensation nuclei measurements: Implications for aerosol indirect effect evaluation. Geophys Res Lett. 46, 14185-14194.

Wang, Y., Wu, Z., Hu, M., 2017. Hygroscopic characteristics of submicron particles under different atmospheric conditions in China. China Environ Sci. 5, 1601-1609. (In Chinese with English abstract)

Wang, Z., Hu, W., Niu, H., Hu, W., Wu, Y., Wu, L., Ren, L., Deng, J., Guo, S., Wu, Z., Zhang, D., Fu, P., Hu, M., 2021b. Variations in physicochemical properties of airborne particles during a heavy haze-to-dust episode in Beijing. Sci Total Environ. 762, 143081.

Wiedensohler, A., Andrade, M., Weinhold, K., Mueller, T., Birmili, W., Velarde, F., Moreno, I., Forno, R., Sanchez, M.F., Laj, P., Ginot, P., Whiteman, D.N., Krejci, R., Sellegri, K., Reichler, T., 2018. Black carbon emission and transport mechanisms to the free troposphere at the La Paz/El Alto (Bolivia) metropolitan area based on the Day of Census (2012). Atmos Environ. 194, 158-169.

Wu, J., Cheng, W., Lu, H., Shi, Y., He, Y., 2018. The effect of particulate matter on visibility in hangzhou, China. J Environ Sci Manag. 21, 100-109.

Wu, Z., Zheng, J., Wang, Y., Shang, D., Du, Z., Zhang, Y., Hu, M., 2017. Chemical and physical properties of biomass burning aerosols and their CCN activity: A case study in Beijing, China. Sci Total Environ. 579, 1260-1268.

Xiao, S., Wang, Q.Y., Cao, J.J., Huang, R.J., Chen, W.D., Han, Y.M., Xu, H.M., Liu, S.X., Zhou, Y.Q., Wang, P., Zhang, J.Q., Zhan, C.L., 2014. Long term trends in visibility and impacts of aerosol composition on visibility impairment in Baoji, China. Atmos Res. 149, 88-95.

Xing, J., 2018. Study on characteristics and aging mechanism of individual particles in $PM_{2.5}$ from Motor vehicle emission. Ph D thesis of China University of Mining & Technology, Beijing. (In Chinese with English abstract)

Xing, J., Shao, L., Zhang, W., Peng, J., Wang, W., Hou, C., Shuai, S., Hu, M., Zhang, D., 2019. Morphology and composition of particles emitted from a port fuel injection gasoline vehicle under real-world driving test cycles. J Environ Sci. 76, 339-

348.

Xing, J., Shao, L., Zhang, W., Peng, J., Wang, W., Shuai, S., Hu, M., Zhang, D., 2020. Morphology and size of the particles emitted from a gasoline direct injection engine vehicle and their ageing in an environmental chamber. Atmos Chem Phys. 20, 2781-2794.

Xing, J., Shao, L., Zheng, R., Peng, J., Wang, W., Guo, Q., Wang, Y., Qin, Y., Shuai, S., Hu, M., 2017. Individual particles emitted from gasoline engines: Impact of engine types, engine loads and fuel components. J Clean Prod. 149, 461-471.

Xu, L., Zhang, D., Li, W., 2019. Microscopic comparison of aerosol particles collected at an urban site in North China and a coastal site in Japan. Sci Total Environ. 669, 948-954.

Xue, T., Liu, J., Zhang, Q., Geng, G., Zheng, Y., Tong, D., Liu, Z., Guan, D., Bo, Y., Zhu, T., He, K., Hao, J., 2019. Rapid improvement of $PM_{2.5}$ pollution and associated health benefits in China during 2013-2017. Sci China Earth Sci. 62, 1847-1856.

Yamato, M., Tanaka, H.J.J.o.G.R.A., 1994. Aircraft observations of aerosols in the free marine troposphere over the North Pacific Ocean: Particle chemistry in relation to air mass origin. J Geophys Res-Atmos. 99, 5353-5377.

Yang, S., Yu, X., Zhao, X., Li, Y., Shun, H., Tian, Z., Li, Y., Wu, S., Wang, Z., 2018. Characteristics of key size spectrum of $PM_{2.5}$ affecting winter haze pollution in taiyuan. Environmental Science. 39, 2512-2520.

Yu, H., Li, W., Zhang, Y., Tunved, P., Dall'Osto, M., Shen, X., Sun, J., Zhang, X., Zhang, J., Shi, Z., 2019. Organic coating on sulfate and soot particles during late summer in the Svalbard Archipelago. Atmos Chem Phys. 19, 10433-10446.

Yuan, Q., Wan, X., Cong, Z., Li, M., Liu, L., Shu, S., Liu, R., Xu, L., Zhang, J., Ding, X., Li, W., 2020. In situ observations of light absorbing carbonaceous aerosols at Himalaya: Analysis of the South Asian sources and Trans-Himalayan Valleys transport pathways. J Geophys Res-Atmos. 125, e2020JD032615.

Yuan, Q., Xu, J., Wang, Y., Zhang, X., Pang, Y., Liu, L., Bi, L., Kang, S., Li, W., 2019. Mixing state and fractal dimension of soot particles at a remote site in the

Southeastern Tibetan Plateau. Environ Sci Technol. 53, 8227-8234.

Yuan, Q., Xu, J.Z., Liu, L., Zhang, A.X., Liu, Y.M., Zhang, J., Wan, X., Li, M.M., Qin, K., Cong, Z.Y., Wang, Y.H., Kang, S.C., Shi, Z.B., Posfai, M., Li, W.J., 2021. Evidence for large amounts of brown carbonaceous tarballs in the Himalayan atmosphere. Environ Sci Tech Let. 8, 16-23.

Yue, S., Ren, L., Song, T., Li, L., Xie, Q., Li, W., Kang, M., Zhao, W., Wei, L., Ren, H., Sun, Y., Wang, Z., Ellam, R.M., Liu, C.Q., Kawamura, K., Fu, P., 2019. Abundance and diurnal trends of fluorescent bioaerosols in the troposphere over Mt. Tai, China, in Spring. J Geophys Res-Atmos. 124, 4158-4173.

Yue, W., Lia, X., Liu, J., Li, Y., Yu, X., Deng, B., Wan, T., Zhang, G., Huang, Y., He, W., Hua, W., Shao, L., Li, W., Yang, S., 2006. Characterization of $PM_{2.5}$ in the ambient air of Shanghai city by analyzing individual particles. Sci Total Environ. 368, 916-925.

Zalakeviciute, R., Alexandrino, K., Rybarczyk, Y., Debut, A., Vizuete, K., Diaz, M., 2020. Seasonal variations in PM_{10} inorganic composition in the Andean City. Sci Rep-UK. 10, 17049.

Zhang, D.Z., Zhao, C.S., Qing, Y., 1998. Analysis of composition and morphology of dust particles. Acta Scientiae Circumstantiae. 18, 3-10. (In Chinese with English abstract)

Zhang, D.Z., Shi, G.Y., Iwasaka, Y., Hu, M., 2000. Mixture of sulfate and nitrate in coastal atmospheric aerosols: individual particle studies in Qingdao (36 degrees 04 ' N, 120 degrees 21 ' E), China. Atmos Environ. 34, 2669-2679.

Zhang, J., Liu, L., Wang, Y., Ren, Y., Wang, X., Shi, Z., Zhang, D., Che, H., Zhao, H., Liu, Y., Niu, H., Chen, J., Zhang, X., Lingaswamy, A.P., Wang, Z., Li, W., 2017. Chemical composition, source, and process of urban aerosols during winter haze formation in Northeast China. Environ Pollut. 231, 357-366.

Zhang, J., Liu, L., Xu, L., Lin, Q., Zhao, H., Wang, Z., Guo, S., Hu, M., Liu, D., Shi, Z., Huang, D., Li, W., 2020a. Exploring wintertime regional haze in northeast China: role of coal and biomass burning. Atmos Chem Phys. 20, 5355-5372.

Zhang, R., Khalizov, A.F., Pagels, J., Zhang, D., Xue, H., McMurry, P.H., 2008. Variability in morphology, hygroscopicity, and optical properties of soot aerosols during atmospheric processing. P Natl Acad Sci USA. 105, 10291-10296.

Zhang, S., Xu, L., Guo, X., Huang, D., Li, W., 2020b. Effects of secondary organic aerosol shells on the hygroscopicity of sodium chloride nuclei: Based on a single particle microscale. Environ Sci. 41, 2017-2025. (In Chinese with English abstract)

Zhang, Y., Yuan, Q., Huang, D., Kong, S., Zhang, J., Wang, X., Lu, C., Shi, Z., Zhang, X., Sun, Y., Wang, Z., Shao, L., Zhu, J., Li, W., 2018. Direct observations of fine primary particles from residential coal burning: insights into their morphology, composition, and hygroscopicity. J Geophys Res-Atmos. 123, 12964-12979.

Zhao, W., Fu, P., Yue, S., Li, L., Xie, Q., Zhu, C., Wei, L., Ren, H., Li, P., Li, W., Sun, Y., Wang, Z., Kawamura, K., Chen, J., 2019. Excitation emission matrix fluorescence, molecular characterization and compound-specific stable carbon isotopic composition of dissolved organic matter in cloud water over Mt. Tai. Atmos Environ. 213, 608-619.

Zhao, Z., Wang, Q., Xu, B., Shen, Z., Huang, R., Zhu, C., Su, X., Zhao, S., Long, X., Liu, S., Cao, J., 2017. Black carbon aerosol and its radiative impact at a high-altitude remote site on the southeastern Tibet Plateau. J Geophys Res-Atmos. 122, 5515-5530.

Zhong, C., Zhou, Y., Smith, K.R., Kennedy, I.M., Chen, C., Aust, A.E., Pinkerton, K.E., 2010. Oxidative injury in the lungs of neonatal rats following short term exposure to ultrafine iron and soot particles. J Toxicol Env Heal A. 73, 837-847.

Zhu, C., Qu, Y., Zhou, Y., Huang, H., Liu, H., Yang, L., Wang, Q., Hansen, A.D.A., Cao, J., 2021. High light absorption and radiative forcing contributions of primary brown carbon and black carbon to urban aerosol. Gondwana Res. 90, 159-164.

Zieger, P., Vaisanen, O., Corbin, J.C., Partridge, D.G., Bastelberger, S., Mousavi Fard, M., Rosati, B., Gysel, M., Krieger, U.K., Leck, C., Nenes, A., Riipinen, I., Virtanen, A., Salter, M.E., 2017. Revising the hygroscopicity of inorganic sea salt particles. Nat Commun. 8, 15883.

Figure Captions

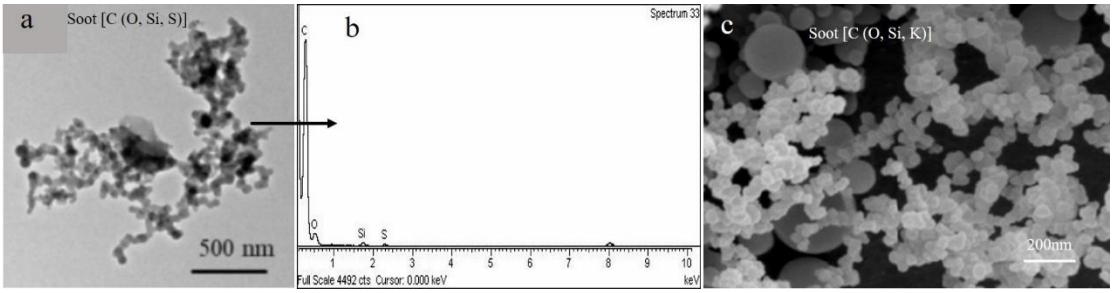

Figure 1. Electron microscopy images of soot particles. a Soot particles observed under TEM, from $PM_{2.5}$ collected in Beijing air 2016. b EDX spectrum of individual soot particle shown in a, c Soot particle observed in SEM, from PM_{10} collected at a coal burning site in Beijing, 2001. a and b are from Wang (2020) and c is from Shao et al. (2006b).

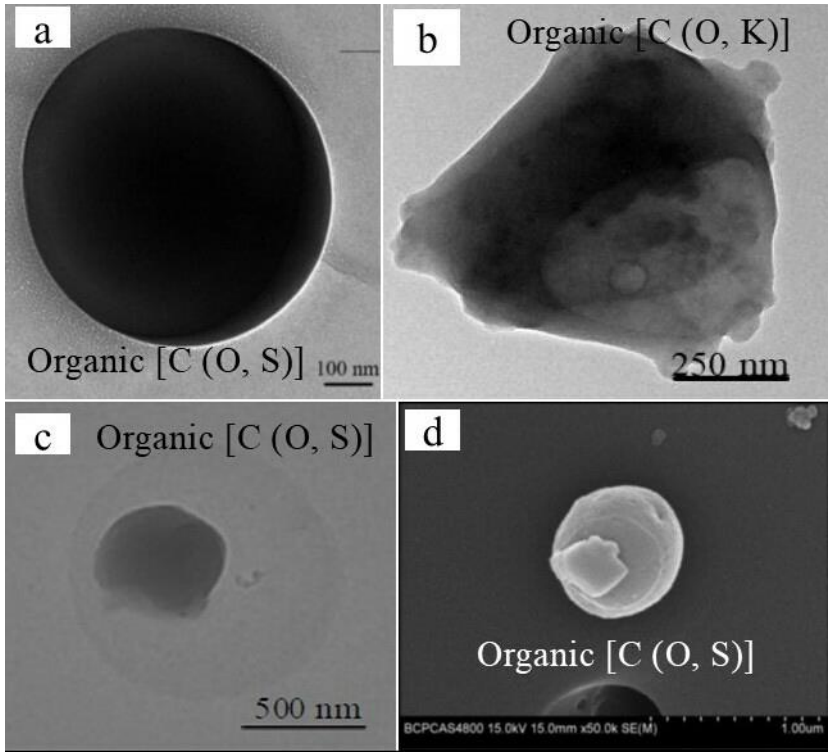

Figure 2. Electron microscopy images of organic particles. a Organic particle (TEM) from $PM_{2.5}$ collected in a tunnel environment in Shenzhen 2014, b Organic particle with irregular shape (TEM) from $PM_{2.5}$ collected in winter in Beijing, c Organic particle in

core-shell structure (TEM) from $PM_{2.5}$ collected in tunnel environment in Shenzhen 2014, d Organic particles in core shell structure shape (SEM) from $PM_{2.5}$ collected in winter in Beijing. a and d are from Hou (2017) and b and c are from Wang (2020).

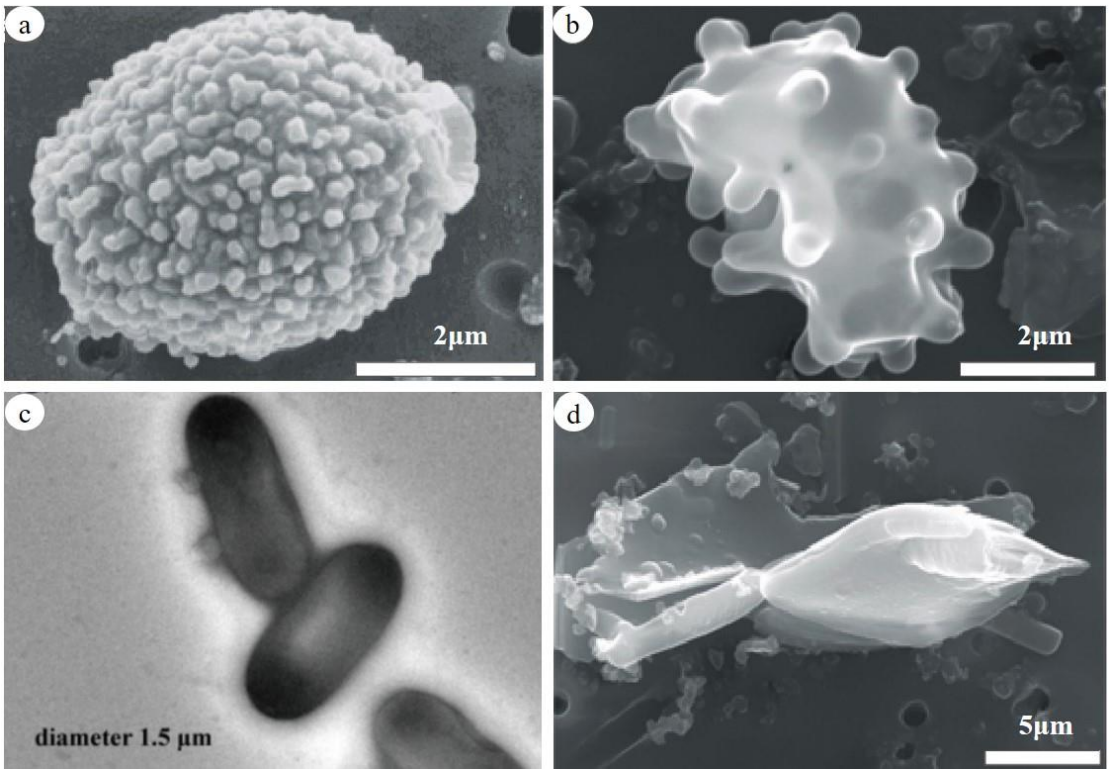

Figure 3. SEM images of biological particles. a. b spores, c bacteria, d plant debris. The images of a, b and d were from samples collected in Beijing in summer 2001 (Shao et al., 2006b, reproduced with permission) and c was from PM2.5 collected in the Lesser Khingan Mountain boreal forest of China (Li et al., 2020a, reproduced with permission).

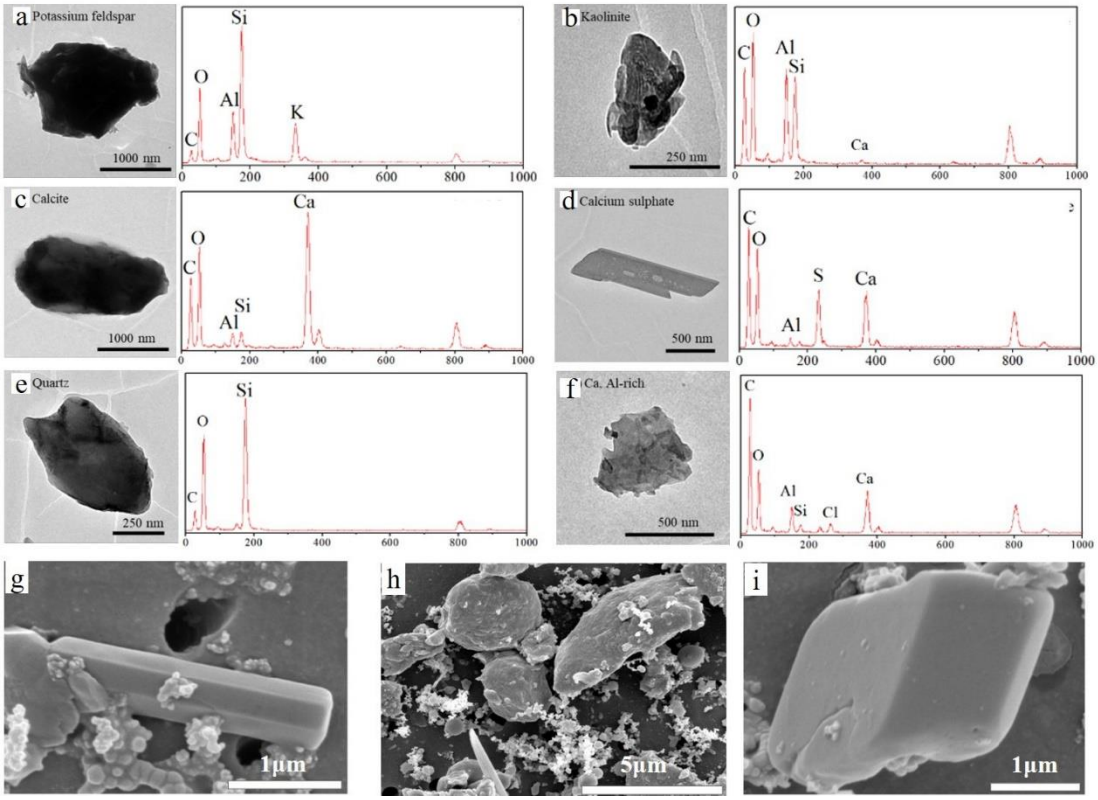

Figure 4. Electron microscopy images of mineral particles. a, Potassium feldspar mineral (TEM), b Kaolinite mineral (TEM), c Calcite mineral (TEM), d Calcium sulphate mineral (TEM), e Quartz mineral (TEM), f Ca, Al-rich mineral (TEM), g Mineral particle in Long-axis shape (SEM), h Mineral particle in irregular shape (SEM), i Mineral particle in regular shape. The images a-f were from $PM_{2.5}$ samples collected in Beijing during two severe dust storms in spring 2015. The images g-i were from PM_{10} samples collected in Beijing in summer 2001. a, b, c, d, e, and f, are from Wang et al. (2021a, reproduced with permission) and g, h and i are from Shao et al. (2006b).

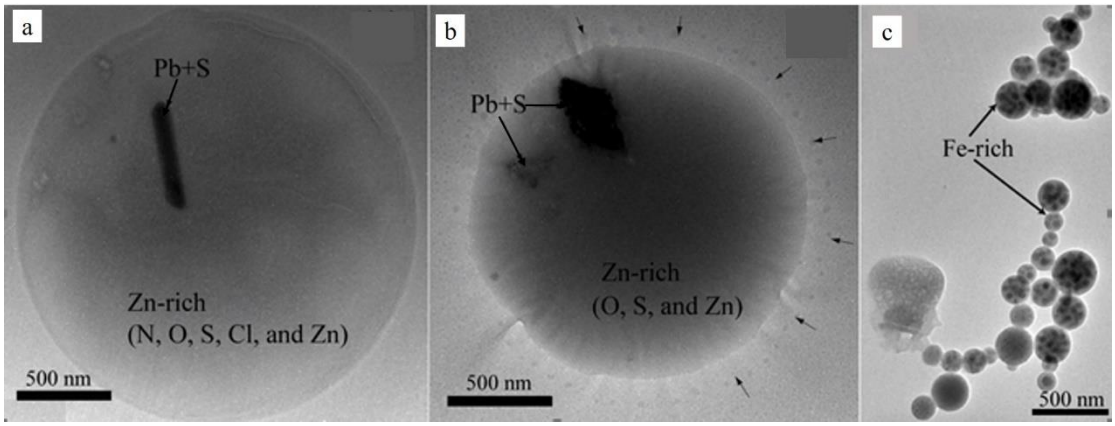

Figure 5. TEM images of metal particles. Elements of the detected parts of individual particles are in parentheses. (a) Zn-rich coatings with a rectangular Pb-rich inclusion, (b) Zn-rich coatings with quadrangular Pb-rich inclusions. (c) Aggregates of spherical Fe-rich particles. The images are from $PM_{2.5}$ samples collected in the haze episodes over northern China, 2007 (Li and Shao, 2009a).

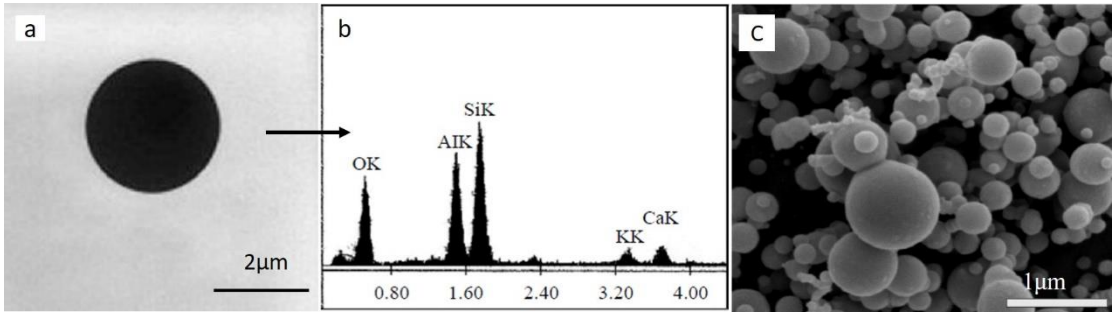

Figure 6. Electron microscopy images of fly ash particles. a The TEM image of a fly ash particle was from $PM_{2.5}$ collected in Beijing in spring 2011. b EDX spectrum of individual fly ash particle shown in a, c The SEM image of fly ash particles from PM_{10} collected at the coking plants in Beijing. a and b are from Li et al. (2013b) and c is from Shao et al. (2016b).

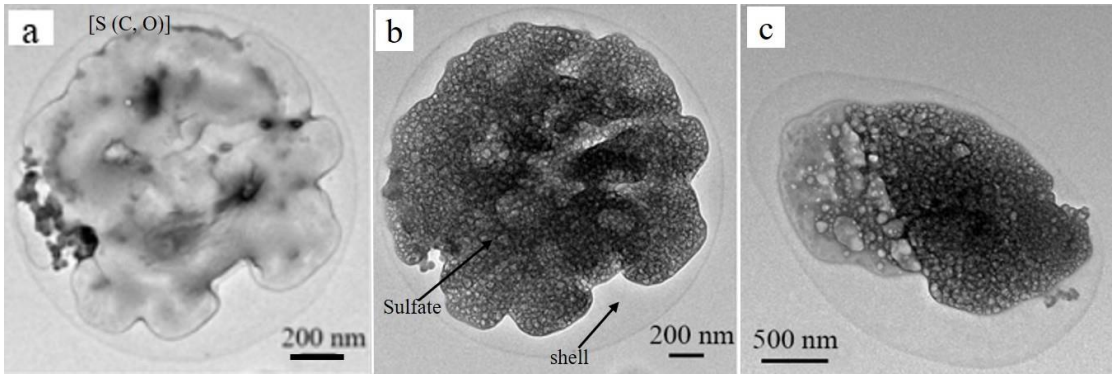

Figure 7. TEM images of sulfate particles. a Sulfate particle in foam-like' structure shape, b and c Sulfate particles with core-shell structure shapes. The images were from $PM_{2.5}$ collected in a tunnel environment in Shenzhen 2014 (Hou, 2017).

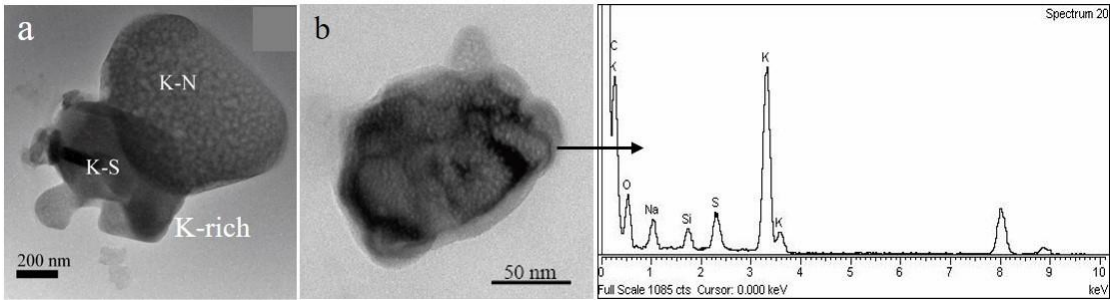

Figure 8. TEM image and EDX spectrum of K-rich particles. Image a was from $PM_{2.5}$ collected in the haze episodes over northern China, 2007 (Li and Shao, 2009a). Image b is from $PM_{2.5}$ collected from a bench experiment of biomass burning (Li, 2021).

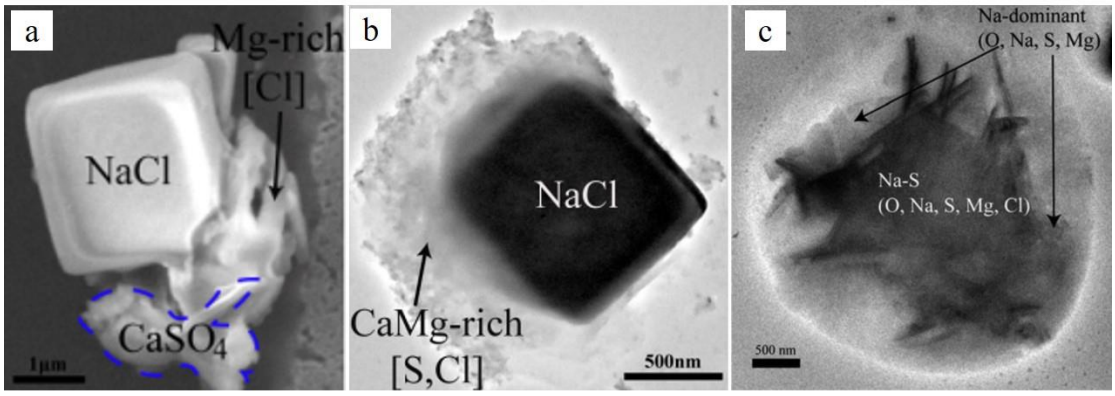

Figure 9. Electron microscopy images of sea salt particles. a A fresh NaCl particle observed in SEM, from aerosol sample collected in Svalbard in summer 2012. b A fresh NaCl particle observed in TEM, from aerosol sample collected in Svalbard in summer 2012, c Amorphous NaCl particles were from aerosol sample collected in a south China coastal city. a and b are from Chi et al. (2015) and c is from Li et al. (2010a, reproduced with permission).

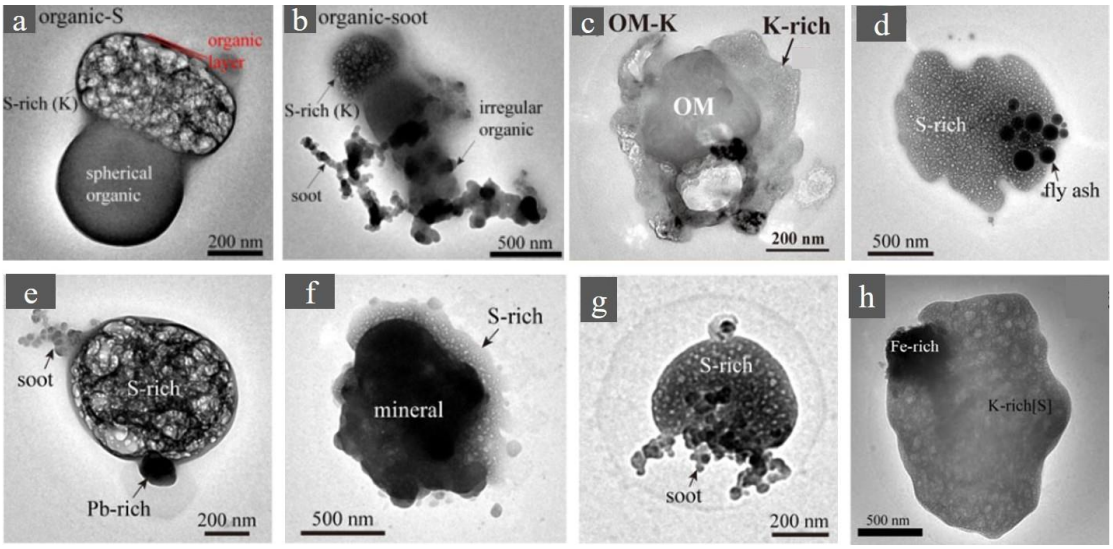

Figure 10. TEM images of some mixed particles. an organic and S-rich mixed particle was from $PM_{2.5}$ collected in haze episodes in in Northeast China (Zhang et al., 2017, reproduced with permission), b organic and soot mixed particle was from $PM_{2.5}$ collected in haze episodes in in Northeast China (Zhang et al., 2017, reproduced with permission), c organic and K-rich mixed particle was from aerosol sample collected in crop residue, wood, and solid waste combustion in a residential stove (Liu et al., 2017), d S-rich and fly ash mixed particle, e S-rich and metal mixed particle, f S-rich and mineral mixed particle, g S-rich and soot mixed particle, d-g were from $PM_{2.5}$ collected at a mountain site in North China 2014 (Liu et al., 2018), (h) K-rich and metal mixed particle were from aerosol sample collected in dust episodes over northern China 2007 (Li and Shao, 2009b). All are mixed particles of irregular shape, except for g which is the mixed particle of core-shell structure.

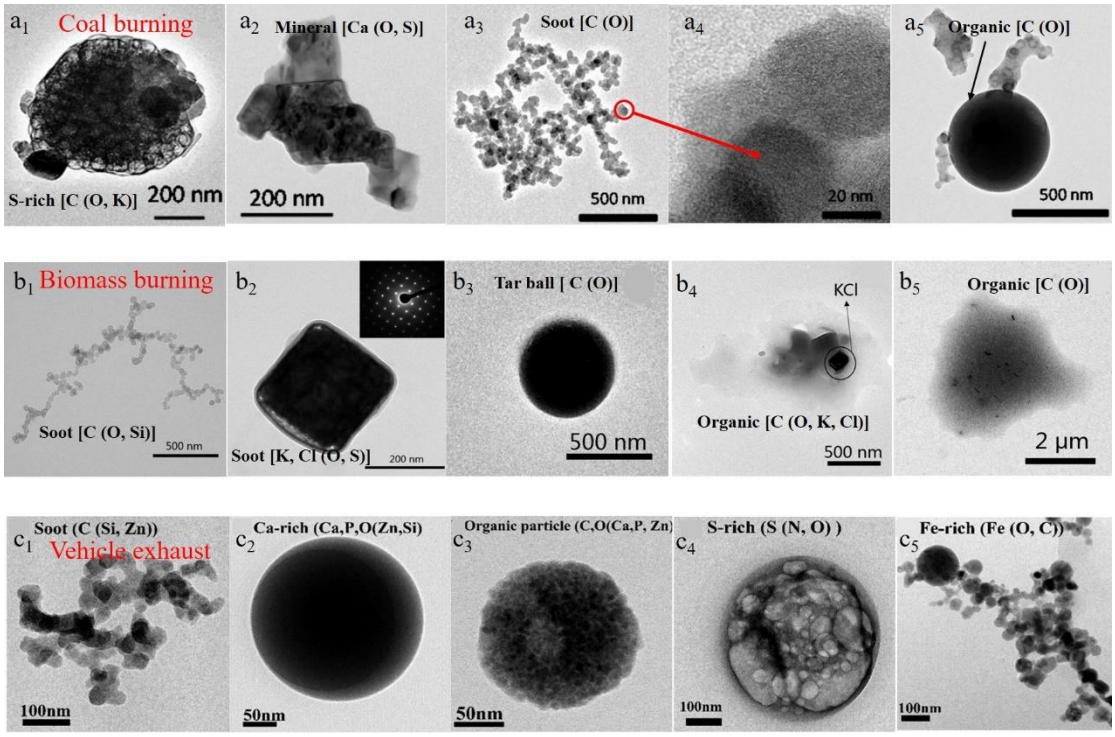

Figure 11. Electron microscopy images of individual particles from the bench experiments of coal burning, biomass burning and vehicle exhaust. a_1-a_5 represent the particles emitted by coal burning, b_1-b_5 represent particles emitted by biomass burning, c_1-c_4 represent particles emitted by vehicle exhaust. a_1, c_4 S-rich particle, a_2 mineral particle, a_3, b_1, c_1 soot particle, a_4 Onion like structure of soot particle at high resolution, a_5, b_5, c_3 organic particle; b_2 K-rich particle, b_3 tar ball, b_4 organic containing k particle, c_2 Ca-rich particle, c_5 Fe-rich particle. The images of a_1 to a_5 are from Wang et al. (2019a). The images of b_1 to b_5 are from Li (2021). The images of c_1 to c_5 are from Xing (2018).

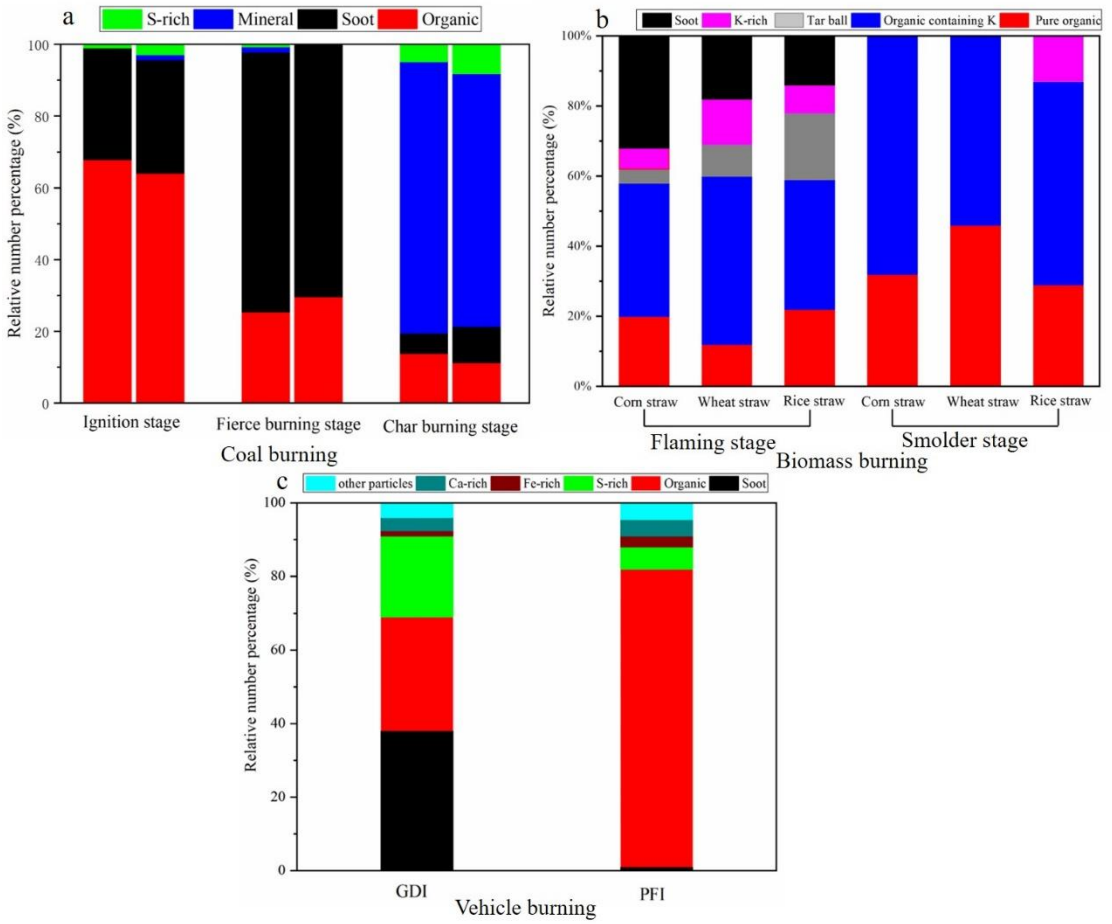

Figure 12. The relative percentage contents of different individual particle types were tested on the bench experiments of coal burning (a), biomass burning (b) and vehicle exhaust (c). a, Coal-burning included the stages of ignition, fierce burning and char burning. b, Three types of straw in the flaming and smoldering stage. c, Vehicle exhaust included emissions from two engine types of GDI (gasoline-direct-injection) and PFI (port fuel injection). The data for image a are from Wang et al. (2019a). The data for image b are from Li (2021). The data for image c are from Xing (2018).

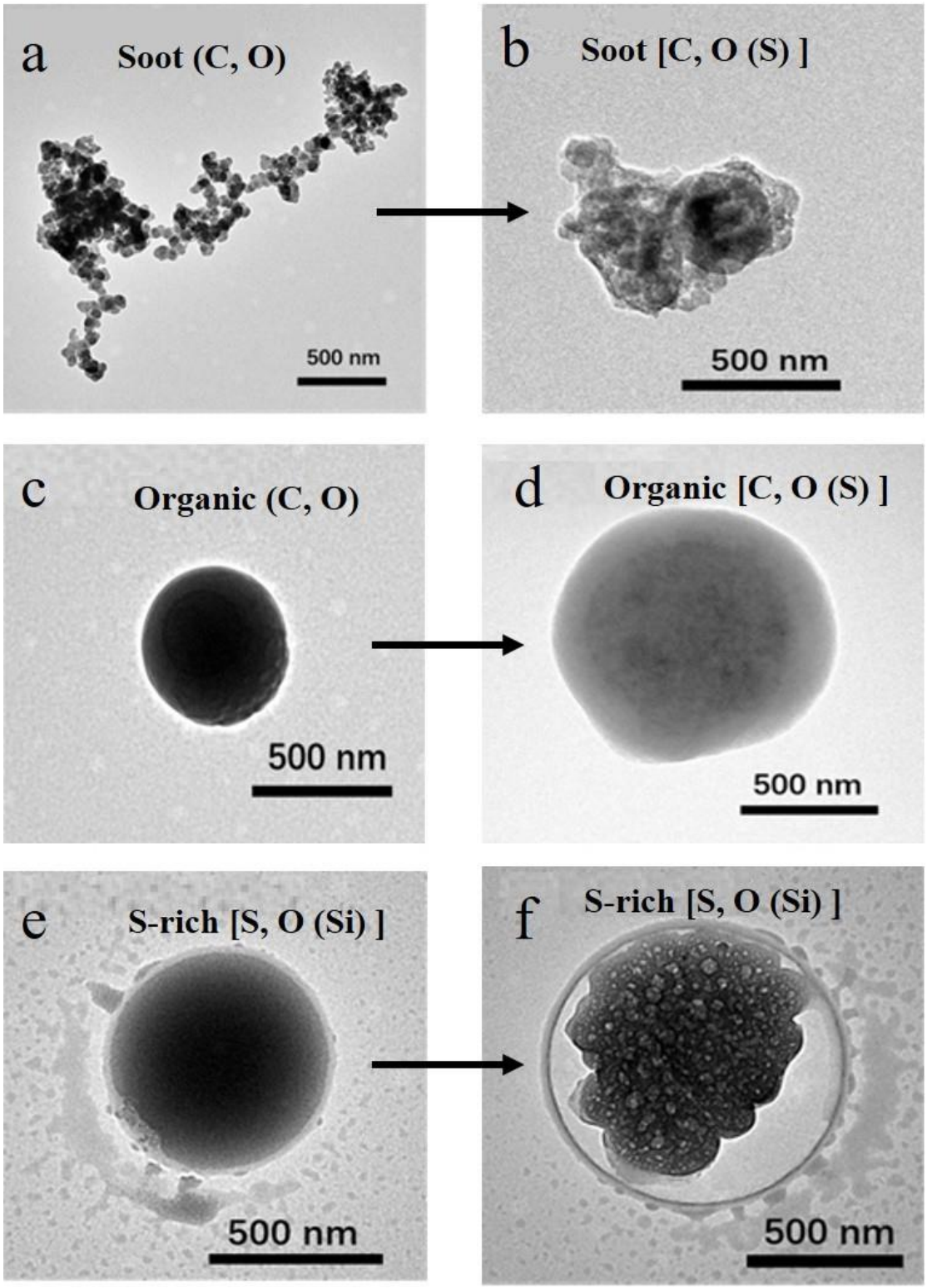

Figure 13. Electron microscopy (TEM) images of individual particles (fresh and aged) from coal burning in smog chamber experiment. a Fresh soot particle; b Aged soot particles; c Fresh organic particle; d Aged organic particle; e Fresh sulfate particle; f Aged sulfate particle. The images are from Li (2021).

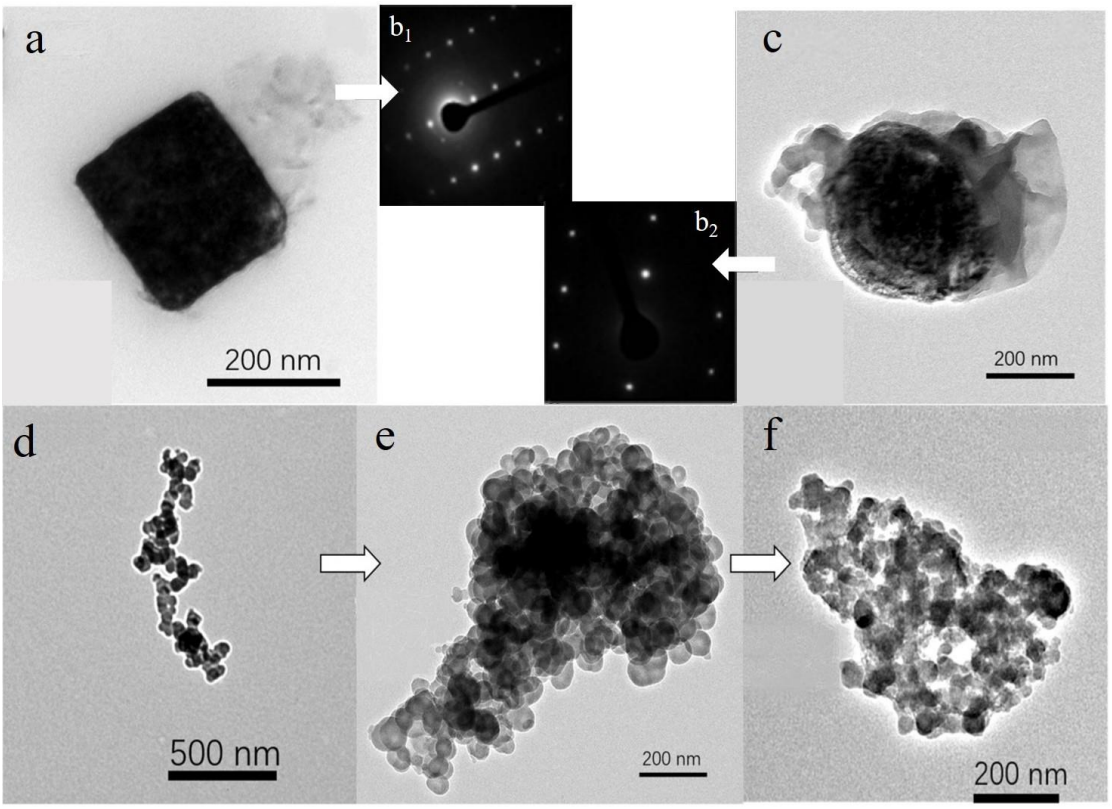

Figure 14. Electron microscopy (TEM) images of individual particles (fresh and aged) from biomass burning in a smog chamber experiment. a KCl particles, b_1 Selected area electron diffraction of a, b_2 Selected area electron diffraction of c, c Amorphous KCl particles, d, e and f soot particles. The images are from Li (2021).

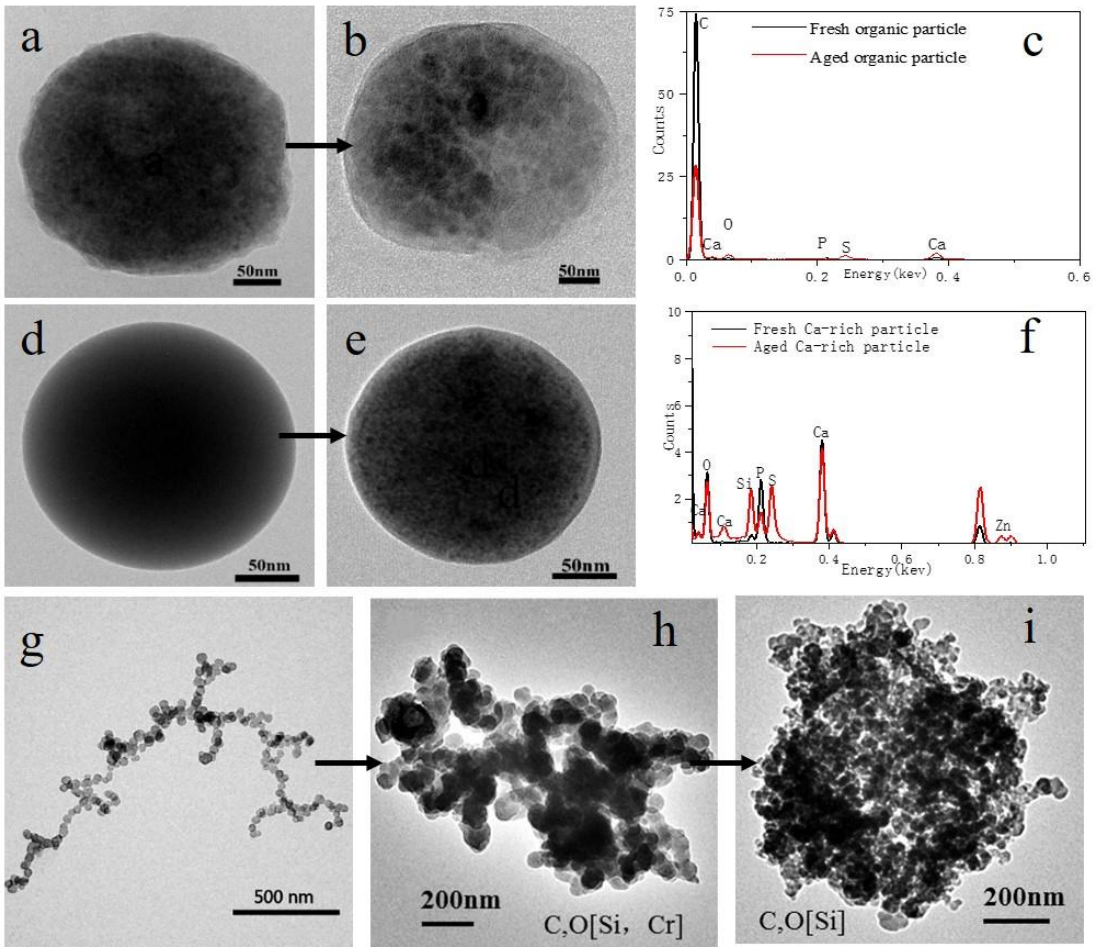

Figure 15. Electron microscopy (TEM) images of individual particles (fresh and aged) from vehicle exhaust in a smog chamber experiment. a Fresh organic particle, b Aged organic particle, c EDX spectra of fresh and aged organic particles, d Fresh Ca-rich particle, e Aged Ca-rich particle, f EDX spectra of fresh and aged particles. g, h, i Soot particles. The images a-h are from Xing et al. (2020) and i is from Xing (2018).

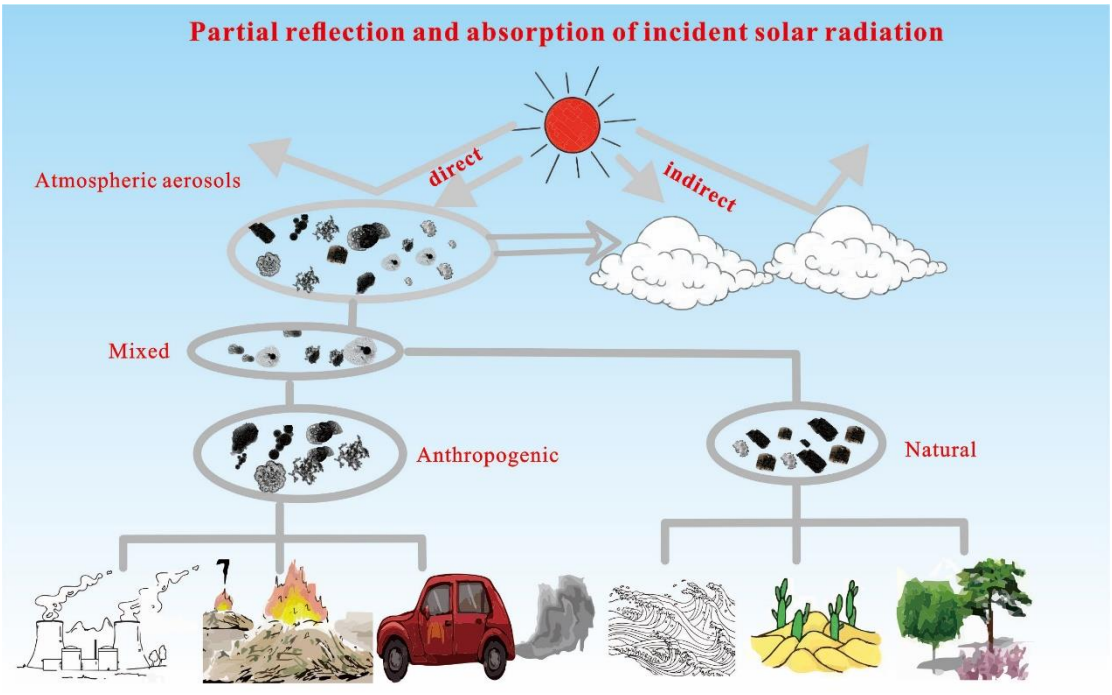

Figure 16. Optical reflection and absorption of aerosols and cloud under incoming solar radiation. Atmospheric particles emitted from natural and anthropogenic sources can mix with each other, and mixed and unmixed particles can directly absorb and reflect solar radiation. Some particles can form CCN that absorb and reflect solar radiation, causing the indirect climate effects.

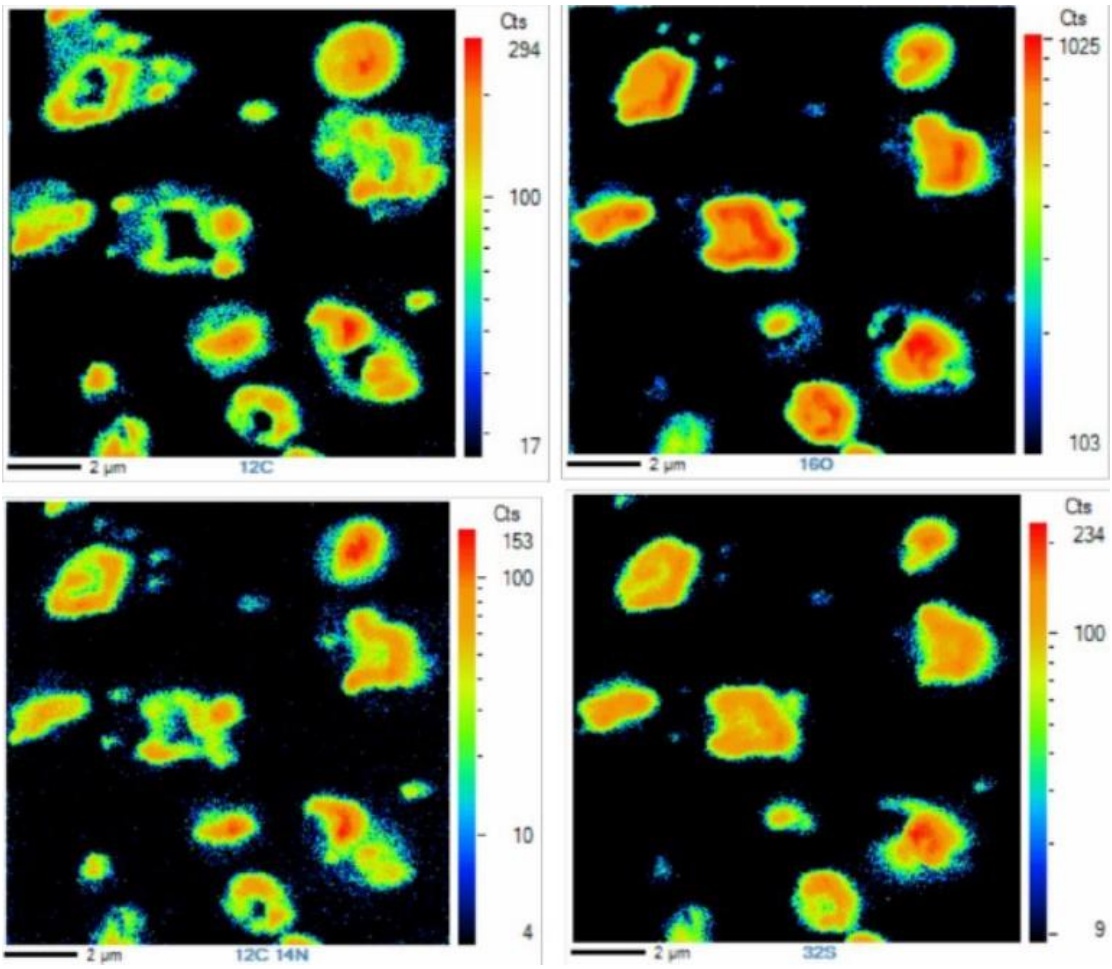

Figure 17. NanoSIMS images of organic and sulfate mixed particles. $C^{14}N^-$ represents the distribution of organic matter content, and $^{32}S^-$ and $^{16}O^-$ represent the distribution of sulfate content in particles. The images were from $PM_{2.5}$ collected at the road in urban Beijing in winter (Xing, 2018).

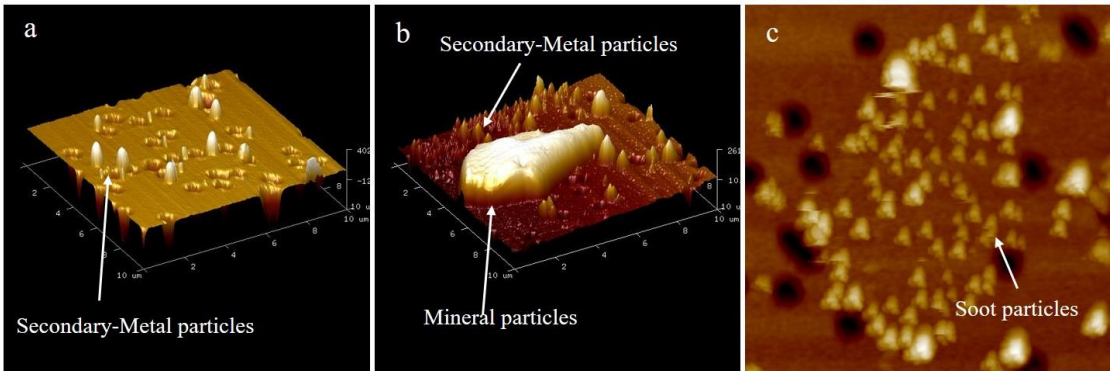

Figure 18. AFM images of particles in $PM_{2.5}$. a Metal and secondary mixed particles, b Mineral particles and secondary mixed particles, c Soot particles. The images were from $PM_{2.5}$ collected in a tunnel environment in Shenzhen 2014 (Hou, 2017). Aerosol species are classified by TEM-EDX analysis.

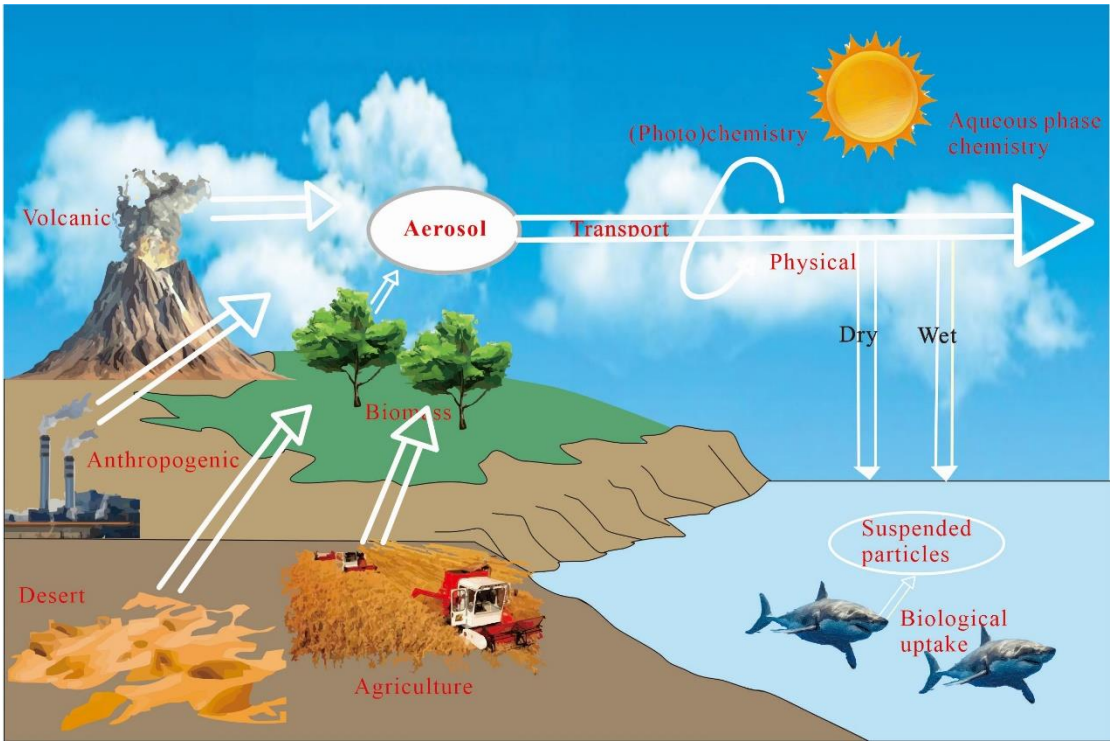

Figure 19. Schematic of aerosols impacts on the ocean. Atmospheric particles emitted by natural and anthropogenic sources can be transported over great distances, affecting local climate and biologicals.

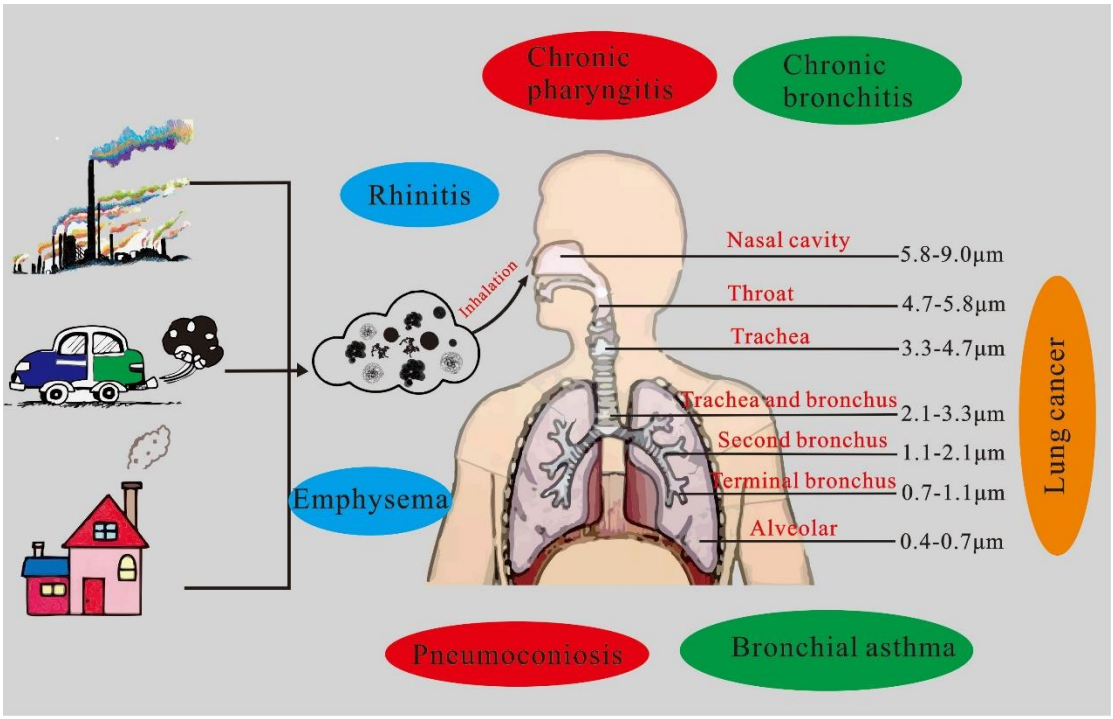

Figure 20. Health risks from exposure to particles in the atmosphere. Airborne particles with different sizes can reach different tissues (Nasal cavity, throat, trachea and bronchus, second bronchus, terminal bronchus and alveolar) in the body and cause corresponding diseases (Rhinitis, chronic pharyngitis, chronic bronchitis, bronchial asthma, pneumoconiosis, emphysema and lung cancer).

1682 **Table Captions**

1683 Table 1 Summary of analytical methods for individual particles

Methods	Size	Morphology	Advantages and drawbacks
Scanning Electron Microscopy (SEM)	best for >100 nm particle	3D particle shape	Low spatial and compositional specificity; only surface information in images
Transmission Electron Microscopy (TEM)	best for <2nm particle	2D particle shape	High spatial specificity for shape, manually operated and labor-intensive, resulting in poor statistics
Surface-Enhanced Raman Scattering (SERS)	best for <10nm particles	No information	The evaporation information of sulfate under vacuum conditions can be observed but no images
Scanning Transmission X-ray Microscopy (STXM-NEXAFS)	best for >100 nm particle	2D particle shape	Specific bond types can be studied in carbonaceous aerosol; synchrotron radiation needed. low spatial resolution
Atomic Force Microscope (AFM)	best for <2nm particle	3D particle shape	The surface texture, viscosity, deformation, and elasticity of the particle can be studied, but the composition of the particle cannot be provided
Nanometer - scale Secondary Ion Mass Spectrometer (Nano – SIMS)	best for >50 nm particle	2D particle shape	Specific bond types can be studied, manually operated and labor-intensive, resulting in poor statistics
Time of Flight Secondary Ion Mass Spectrometer (TOF – SIMS)	best for >100 nm particle	2D particle shape	Specific bond types can be studied; low spatial resolution
Individual Particle Aerosol Mass Spectrometer (SPAMS)	best for >100 nm particles	No information	The chemical composition and particle size of particulate matter can be obtained but no images

	Aerosol-Time-Of-Flight Mass Spectrometer (ATOFMS)/Ultrafine aerosol time-of-flight mass spectrometer (UF-ATOFMS)	ATOFMS, best for >100nm particles UF-ATOFMS, >50nm	No information	Specific bond types can be studied for inorganic and organic particle; online instrument for good statistics but no images
	Micro-Raman Spectroscopy (Micro-RS)	best for >1μm particles	2D particle shape	Direct identification of molecules and functional groups in individual particles; Raman scattering intensity is easily affected by optical system parameters and other factors

1684
1685

1686 Table 2 The types of individual particles in PM2.5 based on TEM-EDX

Categories	Individual particle types		Major element	Morphologies	Major sources
Carbonaceous particles	Soot aggregates		C, O, and minor Si, K	Chain-like, cluster-like, and compact-like morphologies	Emissions from vehicles burning fossil fuel
	Organic particles	Primary organic particles	C and O	Spherical and near-spherical morphologies	Fossil fuel and biomass burning
		Secondary organic particles	C, O, and S	Irregular morphologies	Secondary conversion of volatile organic compounds (VOCs)
	Biological particles		C, O, P, K and Si	Irregular morphologies	Pollen and robes
Non-carbonaceous particles	Mineral particles		Si, Al, Ca, Mg, K, and Fe	Irregular morphologies	Road, construction, and crustal dust
	Metal particles		Zn, Fe, Pb, Mn, and minor Cr	Spherical and irregular morphologies	Coal-fired power plant, heavy industries, and tyre abrasion
	Fly ashes		Si, Al, Fe and minor Na, K	Spherical morphology	Coal combustion
	S-rich particles		S and minor Na, K, Ca	Irregular morphologies and core-shell structure	Derived from SO_2 emitted from coal combustion or vehicles
	K-particles		K, N, S and Cl	Irregular morphologies	Biomass burning
	Sea salt particles		Na, Cl and S	Cubic crystalline morphology	Ocean and blowing snow
Mixed particles	Mixture of above particles		Complicated composition	Irregular morphologies and core-shell structure	Heterogeneous reaction of particles

1687
1688

1689 Table 3 Common types of the internal mixed particles in terms of compositions

organic and sulfate mixed particles
organic and soot mixed particles
organic and K-rich mixed particles
S-rich and fly ash mixed particles
S-rich and metal mixed particles
S-rich and mineral mixed particles
S-rich and soot mixed particles
K-rich and metal mixed particles

1690
1691

Abbreviation

Abbreviation	
ACMS	Aerosol Chemical Speciation Monitoring
AFM	Atomic Force Microscopy
AMS	Aerosol Mass Spectrometry
APPCAP	Air Pollution Prevention and Control Action Plan
ATOFMS	Aerosol-Time-Of-Flight Mass Spectrometry
CCN	Cloud Condensation Nuclei
EDX	Energy Dispersive X-ray Spectroscopy
EPMA	Electron Probe X-ray Micro-Analysis
GDI	Gasoline-Direct-Injection
HPLC/MS	High Performance Liquid Chromatography Mass Spectrometry
IC	Ion Chromatograph
ICP-AES	Inductively Coupled Plasma Atomic Emission Spectrometry
ICP-MS	Inductively Coupled Plasma Mass Spectrometer
ICP-OES	Inductively Coupled Plasma-Optical Emission Spectroscopy
GC-MS	Gas Chromatograph Mass Spectrometry
K-rich	Potassium-rich
Micro-PIXE	Micro-Particle-Induced X-ray Emission
Nano-SIMS	Nanometer-Scale Secondary Ion Mass Spectrometer
NMVOCs	Non-Methane Volatile Organic Compounds
OM	Organic Matter
PFI	Port Fuel Injection
POM	Primary Organic Matter
PTR-MS	Proton Transfer Reaction Mass Spectrometry
SEM	Scanning Electron Microscopy
SERS	Surface-Enhanced Raman Scattering
SOA	Secondary Organic Aerosols
SOM	Secondary Organic Matter
SPAMS	Single Particle Aerosol Mass Spectrometry
STXM	Scanning Transmission X-ray Microscopy
TEM	Transmission Electron Microscopy
TOF-SIMS	Time Of Flight Secondary Ion Mass Spectrometry
VOCs	Volatile Organic Compounds